A dynamic model for the planetary bearings in a double planetary gear set

Jing Liu[1),2)*], Xinbin Li[1),2)], Min Xia[3)]

1) School of Marine Science and Technology, Northwestern Polytechnical University, Xi'an, 710072, People's Republic of China

2) Laboratory for Unmanned Underwater Vehicle, Northwestern Polytechnical University, Xi'an, 710072, People's Republic of China

3) Department of Engineering, Lancaster University, Lancaster, LA1 4YW, United Kingdom

*Corresponding author: Jing Liu. Email: jliu@cqu.edu.cn; jliu0922@nwpu.edu.cn.

Abstract

Double planetary gear sets (DPGSs) are widely applied to high power and high torque mechanical transmission systems due to the high loading capacity, steady transmission, and high transmission efficiency. Most previous works studied the planetary bearing vibration characteristics without the gear excitations. This work establishes a dynamic model for a DPGS containing all components (sun gear, ring gear, carrier, inner planet, outer planet, planetary bearing roller, and planetary bearing cage). The components' excitations in this work are more comprehensive than the reported references. The proposed model considers the planetary bearing roller and cage dynamics. Moreover, the gear interactions, planetary gear-bearing-carrier interactions, and roller-cage interactions are contained in the proposed model. The vibrations of planetary bearing roller, planet, carrier, and planetary bearing cage are analyzed. The effect of sun gear rotation speed on the planetary bearing contact force, planetary bearing roller-cage impact force, and vibrations of planetary bearing parts are studied. The simulated and experimental results are compared to prove the correctness of proposed model. Moreover, the results from proposed model and model without the cage are compared to show the advantage of proposed model.

Keywords: Double planetary gear set (DPGS); planetary bearing; dynamic model; vibrations

1. Introduction

Double planetary gear sets (DPGSs) are widely applied to high power and high torque mechanical transmission systems due to the high loading capacity, steady-transmission, and high transmission efficiency. As one of the key parts of the DPGS, the planetary bearing rotates around the DPGS axis besides its own axis. Due to the special work conditions, the planetary bearings are prone to failure during the operations. The vibrations can reflect the planetary bearing working conditions, which can be helpful for the fault diagnosis and vibration suppression. Thus, it is critical to establish the DPGS dynamic model to analyze the planetary bearing vibrations.

Many studies [1,2] were conducted to research the planetary gear set dynamics. Kahraman [3] studied the planetary gear set (PGS) vibrations by establishing a torsional dynamic model. Parker [4] proposed a two-dimensional dynamic model for PGS. The effect of the tooth profile modification on the PGS vibrations are analyzed in their work [5]. Öztürk et al. [6] proposed a new time-varying meshing stiffness (TVMS) calculation method considering the tooth profile modification to study its' effect on the PGS vibrations. Fatourehchi et al. [7] established a torsional dynamic model to find the best mesh phasing to reduce the PGS vibrations. Chen and Shao [8] proposed a TVMS model considering the ring gear tooth root crack to study its effect on the PGS vibrations. Shen et al. [9] analyzed the effect of the gear wear on the PGS vibrations. In their work, the wear depth is obtained by Archard model, and the effect of the gear wear on the TVMS and gear backlash was considered. Xiang et al. [10] proposed a torsional dynamic model of PGS including the comprehensive gear error, TVMS, and piece-wise backlash nonlinearities. Luo et al. [11] proposed a PGS dynamic model considering the sliding friction between the meshing contact. They analyzed the effect of the spalling defects on the PGS vibrations. Khoozani et al. [12] researched the effect of the gyroscopic effects on the PGS

vibrations. Kim et al. [13] pointed out that the pressures angles and contact ratios will be changed with the time, which will affect the PGS vibrations. Thus, they proposed a PGS dynamic model including the time-varying pressure angles and contact ratios. Xu et al. [14] proposed a TVMS model containing the positioning errors and studied the effect of positioning errors on the PGS vibrations. Hu et al. [15] established a multistage PGS dynamic model and studied the effect of sun gear crack on the PGS vibrations. Wang et al. [16] proposed a DPS-bearing-rotor system dynamic model and analyzed the effect of support bearing misalignments on the system vibrations. The above analysis indicates that most researchers ignored the planetary bearings in dynamic modeling. However, as one of the most important parts in the PGS, the planetary bearing is one of important excitation sources during the actual operations.

The planetary bearing was considered in some studies. Guo and Parker [17] proposed a dynamic model considering the planetary bearing clearance. In their work, the roller was approximated as a spring system; and the roller dynamic characteristics were not considered. Liu et al. [18,19] established a flexible-rigid coupling dynamic model for PGS. They studied the effect of the planetary bearing fault and clearance on the PGS vibrations. Liu et al. [20] developed a dynamic finite element (FE) model for a PGS. They studied the effect of a planetary bearing localized fault on the PGS vibrations. Denni et al. [21] proposed a dynamic model for planetary bearing. In their work, they considered the hydrodynamic lubrication effect in the roller/cage contact. However, the proposed model ignored the effect of the gear meshing excitation. They studied the planetary bearing separately. Moshrefzadeh and Fasana [22] developed a dynamic model for PGS considering the bearing local defect. However, the planetary bearing dynamics were ignored in their work. Based on the above discussions, note that the previous works studied the PGS vibrations ignoring the bearing dynamics, or they studied the planetary bearing vibrations ignoring the gear excitations. However, the planetary bearing is one of the parts of PGS, the planetary bearing vibrations obtained by a dynamic model without the gear excitations are not reasonable. Liu et al. [23,24] studied the effect of the cage flexibility on the bearing skidding dynamic performance under accelerating conditions. Wu et al. [25] studied the distribution of lubricating oil in roller bearing. Besides, the vibration studies for DPGSs are fewer. Thus, it is important to propose a new dynamic model for DPGS including the bearing and gear excitations comprehensively.

This work establishes a dynamic model for DPGS considering the bearing and gear excitations comprehensively. The proposed model considers the planetary bearing roller and cage dynamics. Moreover, the gear interactions, planetary gear-bearing-carrier interactions, and roller-cage interaction are considered in the proposed model. The TVMS is obtained by the method in Ref. [26]. In the proposed method, the mesh deformations are calculated by the gear relative meshing displacements. Moreover, the bearing contact force of two contact parts is calculated by the relative displacement in a Cartesian coordinate system. Besides, the roller-cage impact force is obtained by the relative angular displacement between the roller and cage. The friction moment calculation method in Ref. [27] is used. An experiment is conducted to prove the correctness of proposed model. The effect of the sun gear rotation speed on the planetary bearing vibrations is studied. In comparison with the previous studies, this work establishes an improved dynamic model for DPGS including all components (sun gear, ring gear, carrier, inner planet, outer planet, planetary bearing roller, and planetary bearing cage). The components' excitations in this work are more comprehensive. Moreover, the results frome proposed model and model without the cage are compared to show the advantage of proposed model.

2. Problem description

As one of the key parts of DPGS, the planetary bearing rotates around the DPGS axis besides its own axis. Due to the special work conditions, the planetary bearings are prone to

failure during the operations. However, few studies studied the planetary bearing dynamics and ignored the gear excitations. In the actual operations of a DPGS, the excitations are complicated, which include the gear mesh excitations, TVMS excitations, bearing roller-ring contact excitations, bearing cage-ring impact excitations, and bearing roller-cage impact excitations, as shown in Fig. 1. Thus, the planetary bearing vibrations obtained by the model ignored the gear tooth deformation excitations and TVMS excitations are not reasonable. Thus, an improved dynamic model for DPGS including all components (sun gear, ring gear, carrier, inner planet, outer planet, planetary bearing roller, and planetary bearing cage) is proposed in the following sections.

3. Dynamic modeling of a DPGS

The dynamic models presented in this paper are based on the following assumptions: (1) Each planetary gear is uniformly distributed along the circumference; and their mass and rotational inertia are same. (2) The counterclockwise is defined as the positive direction of rotation. (3) The effect of the gear backlash on the TVMS and mesh deformation are ignored. (4) The flexibilities of components are ignored too.

(a)

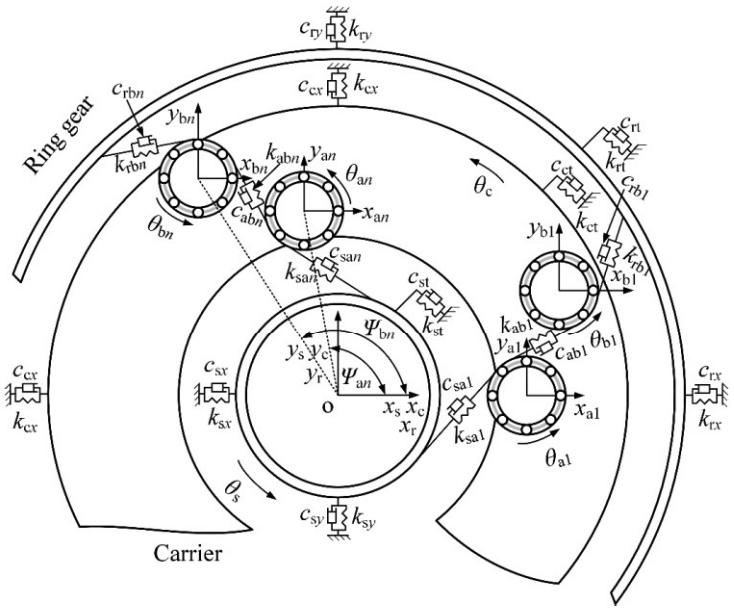

(b)

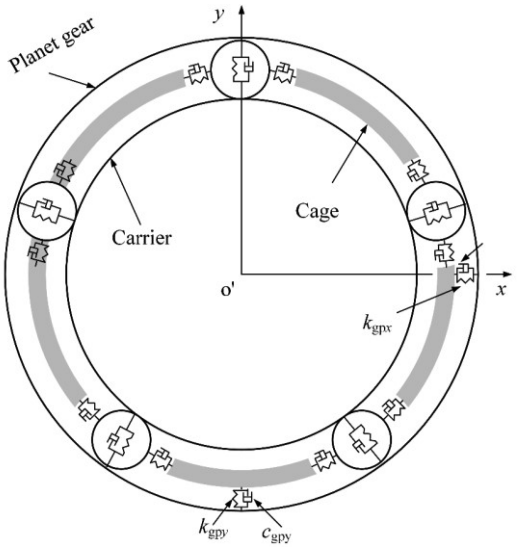

Fig. 1. (a) A dynamic model of DPGS and (b) planetary bearing dynamic model.

Fig. 1 shows the proposed DPGS dynamic model. The DPGS consists of one ring gear (r), one carrier (c), one sun gear (s), *N* inner planet, and *N* outer planetary gear. Three degrees of freedom of each part are considered, which include the transverse movement along the *x*- and *y*-axis, and rotation about the *z*-axis. A fixed coordinate system with the carrier center as the origin, *N* rotating coordinate systems with the inner planetary gear center as the origin, and *N* rotating coordinate systems with the outer planetary gear center as the origin. The rotating coordinate systems rotate around the fixed coordinate system o. In the proposed model, the motion of sun gear, ring gear, and carrier are studied in the fixed coordinate system, the motion of inner/outer planet gears, inner/outer planetary bearing rollers and inner/outer planetary bearing cages are studied in the rotating coordinate systems. The dynamic equations of DPGS are given as follows.

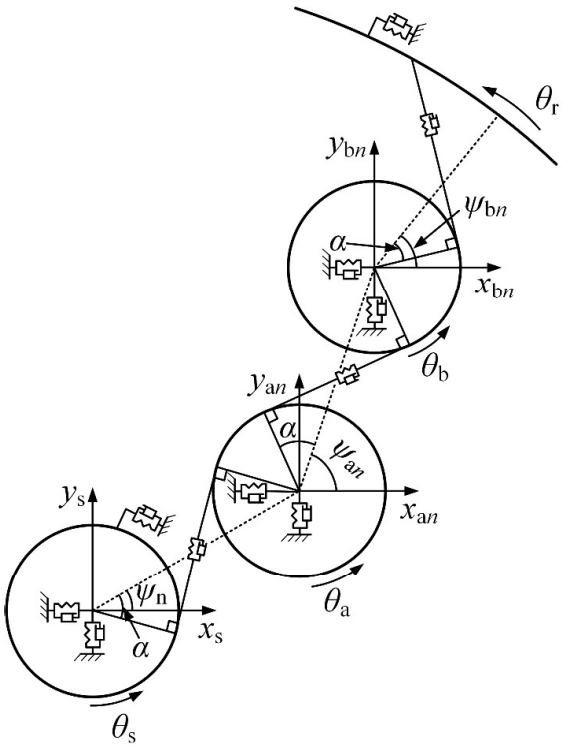

Fig. 2. Gear relative meshing displacements.

The dynamic equations of sun gear are expressed as

$$m_{\mathrm{s}}\ddot{x}_{\mathrm{s}}+c_{\mathrm{s}x}\dot{x}_{\mathrm{s}}+k_{\mathrm{s}x}x_{\mathrm{s}}+\sum F_{\mathrm{sa}n}\cos\psi_{\mathrm{s}n}=m_{\mathrm{s}}x_{\mathrm{s}}\Omega^{2}+2m_{\mathrm{s}}\dot{y}_{\mathrm{s}}\Omega+m_{\mathrm{s}}y_{\mathrm{s}}\dot{\Omega} \tag{1}$$

$$m_{\mathrm{s}}\ddot{y}_{\mathrm{s}}+c_{\mathrm{s}y}\dot{y}_{\mathrm{s}}+k_{\mathrm{s}y}y_{\mathrm{s}}+\sum F_{\mathrm{sa}n}\sin\psi_{\mathrm{s}n}=m_{\mathrm{s}}y_{\mathrm{s}}\Omega^{2}-2m_{\mathrm{s}}\dot{x}_{\mathrm{s}}\Omega-m_{\mathrm{s}}x_{\mathrm{s}}\dot{\Omega} \tag{2}$$

$$\frac{J_{\mathrm{s}}}{r_{\mathrm{s}}}\ddot{\theta}_{\mathrm{s}}+\sum F_{\mathrm{sa}n}=\frac{T_{\mathrm{i}}}{r_{\mathrm{s}}} \tag{3}$$

where, r_{s} is the sun gear base radius; Ω is the carrier rotation velocity; m_{s} is the sun gear mass; $k_{\mathrm{s}x}$ and $c_{\mathrm{s}x}$ are the sun gear bearing stiffness and damping coefficients in x direction; $k_{\mathrm{s}y}$ and $c_{\mathrm{s}y}$ are the sun gear bearing stiffness and damping coefficients in y direction; J_{s} is the sun gear moment of inertia; T_{i} is the DPGS input torque; x_{s} and y_{s} are the sun gear displacements; θ_{s} is the sun gear angular displacement. $F_{\mathrm{sa}n}$ is the nth sun-planet gear mesh force, which is given as

$$F_{\mathrm{sa}n}=k_{\mathrm{sa}n}\delta_{\mathrm{sa}n}+c_{\mathrm{sa}n}\dot{\delta}_{\mathrm{sa}n} \tag{4}$$

where, $k_{\mathrm{sa}n}$ and $c_{\mathrm{sa}n}$ are the nth sun-planet gear mesh stiffness and mesh damping coefficients. The detailed calculation method is given by Ref. [26]. The gear relative meshing displacements is shown in Fig. 2. $\delta_{\mathrm{sa}n}$ is the nth sun-planet gear mesh deformation, which is given as

$$\delta_{\mathrm{sa}n}=\left(x_{\mathrm{s}}-x_{\mathrm{a}n}\right)\cos\psi_{\mathrm{s}n}+\left(y_{\mathrm{s}}-y_{\mathrm{a}n}\right)\sin\psi_{\mathrm{s}n}+r_{\mathrm{s}}\theta_{\mathrm{s}}+r_{\mathrm{a}n}\theta_{\mathrm{a}n}-r_{\mathrm{ac}}\theta_{\mathrm{c}}\cos\alpha \tag{5}$$

$$\psi_{\mathrm{s}n}=\frac{\pi}{2}-\alpha+\psi_{n} \tag{6}$$

where, ψ_n is the nth planet position angle; $r_{\mathrm{a}n}$ is the nth inner planet base radius; r_{ac} is the inner planet mounting radius; θ_{c} is the carrier angular displacement; $x_{\mathrm{a}n}$ and $y_{\mathrm{a}n}$ are the inner planet displacements; $\theta_{\mathrm{a}n}$ is the inner planet angular displacement; α is the pressure angle of gear pair.

The dynamic equations of ring gear are expressed as

$$m_{\mathrm{r}}\ddot{x}_{\mathrm{r}}+c_{\mathrm{r}x}\dot{x}_{\mathrm{r}}+k_{\mathrm{r}x}x_{\mathrm{r}}+\sum F_{\mathrm{rb}n}\cos\psi_{\mathrm{r}n}=m_{\mathrm{r}}x_{\mathrm{r}}\Omega^{2}+2m_{\mathrm{r}}\dot{y}_{\mathrm{r}}\Omega+m_{\mathrm{r}}y_{\mathrm{r}}\dot{\Omega} \tag{7}$$

$$m_{\mathrm{r}}\ddot{y}_{\mathrm{r}}+c_{\mathrm{r}y}\dot{y}_{\mathrm{r}}+k_{\mathrm{r}y}y_{\mathrm{r}}-\sum F_{\mathrm{rb}n}\sin\psi_{\mathrm{r}n}=m_{\mathrm{r}}y_{\mathrm{r}}\Omega^{2}-2m_{\mathrm{r}}\dot{x}_{\mathrm{r}}\Omega-m_{\mathrm{r}}x_{\mathrm{r}}\dot{\Omega} \tag{8}$$

$$\frac{J_{\mathrm{r}}}{r_{\mathrm{r}}}\ddot{\theta}_{\mathrm{r}}+\frac{c_{\mathrm{r}t}}{r_{\mathrm{r}}}\dot{\theta}_{\mathrm{r}}+\frac{k_{\mathrm{r}t}}{r_{\mathrm{r}}}\theta_{\mathrm{r}}-\sum F_{\mathrm{rb}n}=0 \tag{9}$$

where, r_{r} is the ring gear base radius; m_{r} is the ring gear mass; $k_{\mathrm{r}x}$ and $c_{\mathrm{r}x}$ are the ring support stiffness and damping coefficients in x direction; $k_{\mathrm{r}y}$ and $c_{\mathrm{r}y}$ are the ring support stiffness and damping coefficients in y direction; J_{r} is the ring gear moment of inertia; x_{r} and y_{r} are the ring gear displacements; θ_{r} is the ring gear angular displacement. $F_{\mathrm{rb}n}$ is the nth ring-planet gear mesh force, which is given as

$$F_{\mathrm{rb}n}=k_{\mathrm{rb}n}\delta_{\mathrm{rb}n}+c_{\mathrm{rb}n}\dot{\delta}_{\mathrm{rb}n} \tag{10}$$

where, $k_{\mathrm{rb}n}$ and $c_{\mathrm{rb}n}$ are the n-th ring-planet gear mesh stiffness and mesh damping coefficients. $\delta_{\mathrm{rb}n}$ is the nth ring-planet gear mesh deformation, which is given as

$$\delta_{\mathrm{rb}n}=\left(x_{\mathrm{r}}-x_{\mathrm{b}n}\right)\cos\psi_{\mathrm{r}n}+\left(y_{\mathrm{b}n}-y_{\mathrm{r}}\right)\sin\psi_{\mathrm{r}n}+r_{\mathrm{b}}\theta_{\mathrm{b}n}-r_{\mathrm{r}}\theta_{\mathrm{r}n}+r_{\mathrm{a}}\theta_{\mathrm{c}}+r_{\mathrm{r}}\theta_{\mathrm{c}} \tag{11}$$

$$\psi_{\mathrm{r}n}=\frac{\pi}{2}-\alpha+\psi_{\mathrm{b}n} \tag{12}$$

$$\psi_{\mathrm{b}n}=\arccos\frac{\left(Z_{\mathrm{s}}+Z_{\mathrm{a}}\right)^{2}+\left(Z_{\mathrm{r}}-Z_{\mathrm{b}}\right)^{2}-\left(Z_{\mathrm{a}}+Z_{\mathrm{b}}\right)^{2}}{2\left(Z_{\mathrm{s}}+Z_{\mathrm{a}}\right)\left(Z_{\mathrm{r}}-Z_{\mathrm{b}}\right)}+\psi_{n} \tag{13}$$

where, $r_{\mathrm{b}n}$ is the nth outer planet base radius; $x_{\mathrm{b}n}$ and $y_{\mathrm{b}n}$ are the outer planet displacements; $\theta_{\mathrm{b}n}$ is the outer planet angular displacement; Z_{s}, Z_{r}, Z_{a}, and Z_{b} are the teeth numbers of sun gear, ring gear, inner planet, and outer planet, respectively.

The dynamic equations of inner planet are expressed as

$$m_{an}\ddot{x}_{an} = m_{an}x_{an}\Omega^2 + 2m_{an}\dot{y}_{an}\Omega + m_{an}y_{an}\dot{\Omega} + m_{an}r_c\Omega^2\cos\psi_{an} + F_{ax}^{o} + F_{adx}^{o} - F_{agx}^{o} + F_{san}\cos\psi_{sn} - F_{abn}\cos\psi_{abn} \tag{14}$$

$$m_{an}\ddot{y}_{an} = m_{an}y_{an}\Omega^2 - 2m_{an}\dot{x}_{an}\Omega - m_{an}x_{an}\dot{\Omega} + m_{an}r_c\Omega^2\sin\psi_n + F_{y}^{o} + F_{dy}^{o} - F_{agy}^{o} + F_{san}\sin\psi_{sn} - F_{abn}\sin\psi_{abn} \tag{15}$$

$$\frac{J_{an}}{r_{an}}\ddot{\theta}_{an} + F_{san} - F_{abn} + \frac{M_{cage}}{r_{an}} + \frac{\sum f_{aoj}\dfrac{d_m}{2}}{r_{an}} = 0 \tag{16}$$

where, m_{an} is the nth inner planet mass; J_{an} is the nth inner planet moment of inertia; d_m is the inner planetary bearing pitch diameter; M_{cage} is the inner planet-cage friction moment; f_{aoj} is the inner planet-roller friction force; F_{abn} is the nth inner-outer planet gear mesh force; F_{ax}^{o} and F_{ay}^{o} are the resultant forces of inner planet-roller contact force and frictional force in x and y directions; F_{adx}^{o} and F_{ady}^{o} are the inner planet-roller damping forces in x and y directions; F_{agx}^{o} and F_{agy}^{o} are the resultant forces of inner planet-cage impact force and frictional force in x and y directions, which are given by

$$F_{abn} = k_{abn}\delta_{abn} + c_{abn}\dot{\delta}_{abn} \tag{17}$$

$$F_{ax}^{o} = \sum_{j=1}^{Z}\left(Q_{ao}(j)\cos\theta_{aj} + f_{aoj}\sin\theta_{aj}\right) \tag{18}$$

$$F_{ay}^{o} = \sum_{j=1}^{Z}\left(Q_{ao}(j)\sin\theta_{aj} + f_{aoj}\cos\theta_{aj}\right) \tag{19}$$

$$F_{adx}^{o} = \sum c_o\left(\dot{x}_{aej} - \dot{x}_a\right) \tag{20}$$

$$F_{ady}^{o} = \sum c_o\left(\dot{y}_{aej} - \dot{y}_a\right) \tag{21}$$

where, k_{abn} and c_{abn} are the nth inner-outer planet gear mesh stiffness and mesh damping coefficients; c_o is the damping coefficient in the roller-planet contact; x_{ej} and y_{ej} are the jth planetary bearing roller displacements; ϕ_j is the jth roller position angle; the subscript a represents inner planetary bearing; Q_{ao} is the inner planet-roller contact force; f_{ao} is the inner planet-roller friction force; δ_{abn} is the mesh deformation of nth inner-outer planet gear mesh, which are given by

$$\delta_{abn} = \left(x_{an} - x_{bn}\right)\cos\psi_{abn} + \left(y_{an} - y_{bn}\right)\sin\psi_{abn} - r_a\theta_{an} - r_b\theta_{bn} \tag{22}$$

$$\psi_{abn} = -\frac{\pi}{2} + \alpha + \psi_{an} \tag{23}$$

$$\psi_{an} = \arccos\frac{\left(Z_r - Z_b\right)\cos\psi_{bn} - \left(Z_s + Z_a\right)\cos\psi_n}{Z_a + Z_b} \tag{24}$$

$$Q_{ao} = \zeta_{ao}K_o\delta_{ao}^{\frac{10}{9}} \tag{25}$$

$$f_{ao} = \mu Q_{ao} \tag{26}$$

where, ζ_{ao} is the inner planet-roller contact factor, ζ_{ao}=1 when δ_{ao}>0, ζ_{ao}=0 when $\delta_{ao}\leqslant 0$; μ is the friction coefficient, the lubrication condition is considered to be excellent; and the lubrication state is considered to be elastohydrodynamic lubrication in this work. Thus, the friction coefficient can be considered as a constant value and its value is 0.007 in the work; δ_{ao} is the inner planet-roller contact deformation, which is given by

$$\delta_{ao} = \left(x_{aej} - x_a\right)\cos\theta_{aj} + \left(y_{aej} - y_a\right)\sin\theta_{aj} \tag{27}$$

The dynamic equations of outer planet are expressed as

$$\begin{aligned} m_{\mathrm{b}n}\ddot{x}_{\mathrm{b}n} &= m_{\mathrm{b}n}x_{\mathrm{b}n}\Omega^2 + 2m_{\mathrm{b}n}\dot{y}_{\mathrm{b}n}\Omega + m_{\mathrm{b}n}y_{\mathrm{b}n}\dot{\Omega} + m_{\mathrm{b}n}r_{\mathrm{c}}\Omega^2\cos\psi_{\mathrm{b}n} \\ &+F_{\mathrm{b}x}^{\mathrm{o}} + F_{\mathrm{bd}x}^{\mathrm{o}} - F_{\mathrm{bg}x}^{\mathrm{o}} + F_{\mathrm{rb}n}\cos\psi_{\mathrm{r}n} + F_{\mathrm{ab}n}\cos\psi_{\mathrm{ab}n} \end{aligned} \tag{28}$$

$$\begin{aligned} m_{\mathrm{b}n}\ddot{y}_{\mathrm{b}n} &= m_{\mathrm{b}n}y_{\mathrm{b}n}\Omega^2 - 2m_{\mathrm{b}n}\dot{x}_{\mathrm{b}n}\Omega - m_{\mathrm{b}n}x_{\mathrm{b}n}\dot{\Omega} + m_{\mathrm{b}n}r_{\mathrm{bc}}\Omega^2\sin\psi_n \\ &+F_{\mathrm{b}y}^{\mathrm{o}} + F_{\mathrm{bd}y}^{\mathrm{o}} - F_{\mathrm{bg}y}^{\mathrm{o}} - F_{\mathrm{rb}n}\sin\psi_{\mathrm{r}n} + F_{\mathrm{ab}n}\sin\psi_{\mathrm{ab}n} \end{aligned} \tag{29}$$

$$\frac{J_{\mathrm{b}n}}{r_{\mathrm{b}n}}\ddot{\theta}_{\mathrm{b}n} + F_{\mathrm{rb}n} - F_{\mathrm{ab}n} + M_{\mathrm{cage}} + \sum f_{\mathrm{bo}j}\frac{d_{\mathrm{m}}}{2} = 0 \tag{30}$$

where, $m_{\mathrm{b}n}$ is the nth outer planet mass; $J_{\mathrm{b}n}$ is the nth outer planet moment of inertia; $x_{\mathrm{b}n}$ and $y_{\mathrm{b}n}$ are the nth outer planet displacements; $\theta_{\mathrm{b}n}$ is nth outer planet angular displacement; $F_{\mathrm{b}x}^{\mathrm{o}}$ and $F_{\mathrm{b}y}^{\mathrm{o}}$ are the resultant forces of outer planet-roller contact force and frictional force in x and y directions; $F_{\mathrm{bd}x}^{\mathrm{o}}$ and $F_{\mathrm{bd}y}^{\mathrm{o}}$ are the outer planet-roller damping forces in x and y directions; $F_{\mathrm{bg}x}^{\mathrm{o}}$ and $F_{\mathrm{bg}y}^{\mathrm{o}}$ are the resultant forces of outer planet-cage impact force and frictional force in x and y directions; the subscript b represents the outer planetary bearing; the planetary bearing cage is guided by the outer ring and the cage force analysis is shown in Fig. 3. The calculation method of the above variates is given by

$$F_{\mathrm{b}x}^{\mathrm{o}} = \sum_{j=1}^{Z}\left(Q_{\mathrm{bo}}(j)\cos\theta_{\mathrm{b}j} + f_{\mathrm{bo}j}\sin\theta_{\mathrm{b}j}\right) \tag{31}$$

$$F_{\mathrm{b}y}^{\mathrm{o}} = \sum_{j=1}^{Z}\left(Q_{\mathrm{bo}}(j)\sin\theta_{\mathrm{b}j} + f_{\mathrm{bo}j}\cos\theta_{\mathrm{b}j}\right) \tag{32}$$

$$F_{\mathrm{bd}x}^{\mathrm{o}} = \sum c_{\mathrm{o}}\left(\dot{x}_{\mathrm{bc}j} - \dot{x}_{\mathrm{b}}\right) \tag{33}$$

$$F_{\mathrm{bd}y}^{\mathrm{o}} = \sum c_{\mathrm{o}}\left(\dot{y}_{\mathrm{bc}j} - \dot{y}_{\mathrm{b}}\right) \tag{34}$$

$$\begin{bmatrix} F_{\mathrm{g}x} \\ F_{\mathrm{g}y} \\ M_{\mathrm{cage}} \end{bmatrix} = \begin{bmatrix} -\cos\phi_{\mathrm{g}} & -\sin\phi_{\mathrm{g}} & 0 \\ -\sin\phi_{\mathrm{g}} & \cos\phi_{\mathrm{g}} & 0 \\ 0 & 0 & 1 \end{bmatrix}\begin{bmatrix} F_{\mathrm{g}}^{n} \\ F_{\mathrm{g}}^{\tau} \\ M_{\mathrm{g}} \end{bmatrix} \tag{35}$$

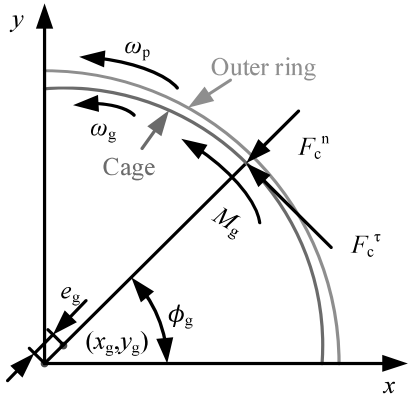

Fig. 3. The force between the cage and guide surface.

where, Q_{bo} is the outer planet-roller contact force; f_{bo} is the outer planet-roller friction force; F_{g}^{n} is the outer planet-cage impact force; c_{o} is the damping coefficient in the roller-planet contact; F_{g}^{τ} is the outer planet-cage friction force; M_{g} is the outer planet-cage friction moment, which are given by

$$Q_{\mathrm{bo}} = \zeta_{\mathrm{bo}}K_{\mathrm{o}}\delta_{\mathrm{bo}}^{\frac{10}{9}} \tag{36}$$

$$f_{\mathrm{ao}} = \mu Q_{\mathrm{ao}} \tag{37}$$

$$F_{\mathrm{g}}^{\mathrm{n}} = K_{\mathrm{g}}\left(e_{\mathrm{g}} - C_{\mathrm{g}}\right) + c_{\mathrm{g}}\dot{e}_{\mathrm{g}} \tag{38}$$

$$F_{\mathrm{g}}^{\tau} = \mu F_{\mathrm{g}}^{\mathrm{n}} \tag{39}$$

$$M_{\mathrm{g}} = F_{\mathrm{g}}^{\tau} R_{\mathrm{cd}} \tag{40}$$

where, ζ_{bo} is the outer planet-roller contact factor, ζ_{bo}=1 when δ_{bo}>0, ζ_{bo}=0 when $\delta_{\mathrm{bo}}\leqslant$0; δ_{bo} is the outer planet-roller contact deformation; K_{o} is the contact stiffness between the roller and outer ring (planet); and e_{g} is the cage center offset, which are given by

$$\delta_{\mathrm{bo}} = \left(x_{\mathrm{be}j} - x_{\mathrm{b}}\right)\cos\phi_{\mathrm{b}j} + \left(y_{\mathrm{be}j} - y_{\mathrm{b}}\right)\sin\phi_{\mathrm{b}j} \tag{41}$$

$$e_{\mathrm{g}} = \sqrt{x_{\mathrm{g}}^2 + y_{\mathrm{g}}^2} \tag{42}$$

The dynamic equations of carrier are expressed as

$$m_{\mathrm{c}}\ddot{x}_{\mathrm{c}} = m_{\mathrm{c}}x_{\mathrm{c}}\Omega^2 + 2m_{\mathrm{c}}\dot{y}_{\mathrm{c}}\Omega + m_{\mathrm{c}}y_{\mathrm{c}}\dot{\Omega} - F_{\mathrm{a}x}^{\mathrm{i}} - F_{\mathrm{da}x}^{\mathrm{i}} - F_{\mathrm{b}x}^{\mathrm{i}} - F_{\mathrm{db}x}^{\mathrm{i}} - c_{\mathrm{c}x}\dot{x}_{\mathrm{c}} - k_{\mathrm{c}x}x_{\mathrm{c}} \tag{43}$$

$$m_{\mathrm{c}}\ddot{y}_{\mathrm{c}} = m_{\mathrm{c}}y_{\mathrm{c}}\Omega^2 - 2m_{\mathrm{c}}\dot{x}_{\mathrm{c}}\Omega - m_{\mathrm{c}}x_{\mathrm{c}}\dot{\Omega} - F_{\mathrm{a}y}^{\mathrm{i}} - F_{\mathrm{da}y}^{\mathrm{i}} - F_{\mathrm{b}y}^{\mathrm{i}} - F_{\mathrm{db}y}^{\mathrm{i}} - c_{\mathrm{c}x}\dot{y}_{\mathrm{c}} - k_{\mathrm{c}x}y_{\mathrm{c}} \tag{44}$$

$$J_{\mathrm{c}}\ddot{\theta}_{\mathrm{c}} + F_{\mathrm{a}x}^{\mathrm{i}}\sin\psi_{n}r_{\mathrm{ac}} + F_{\mathrm{b}x}^{\mathrm{i}}\sin\psi_{\mathrm{b}n}r_{\mathrm{bc}} - F_{\mathrm{a}y}^{\mathrm{i}}\cos\psi_{\mathrm{a}n}r_{\mathrm{ac}} - F_{\mathrm{b}y}^{\mathrm{i}}\cos\psi_{\mathrm{b}n}r_{\mathrm{bc}} = T_0 \tag{45}$$

where, m_{c} is the carrier mass; J_{c} is the carrier moment of inertia; x_{c} and y_{c} are the carrier displacements; θ_{c} is the carrier angular displacement; $F_{\mathrm{a/b}x}^{\mathrm{i}}$ and $F_{\mathrm{a/b}y}^{\mathrm{i}}$ are the resultant forces of inner/outer planetary bearing roller-carrier contact force and frictional force in x and y directions; $F_{\mathrm{a/bd}x}^{\mathrm{i}}$ and $F_{\mathrm{a/bd}y}^{\mathrm{i}}$ are the inner/outer planetary bearing roller-carrier damping forces in x and y directions, which are given by

$$F_{\mathrm{a/b}x}^{\mathrm{i}} = \sum_{j=1}^{Z}\left(Q_{\mathrm{a/bi}}\left(j\right)\cos\theta_{\mathrm{a/b}j} + f_{\mathrm{a/bi}j}\sin\theta_{\mathrm{a/b}j}\right) \tag{46}$$

$$F_{\mathrm{a/b}y}^{\mathrm{i}} = \sum_{j=1}^{Z}\left(Q_{\mathrm{a/bi}}\left(j\right)\sin\theta_{\mathrm{a/b}j} + f_{\mathrm{a/bi}j}\cos\theta_{\mathrm{a/b}j}\right) \tag{47}$$

$$F_{\mathrm{a/bd}x}^{\mathrm{i}} = \sum c_{\mathrm{i}}\left(\dot{x}_{\mathrm{c}} - \dot{x}_{\mathrm{a/be}j}\right) \tag{48}$$

$$F_{\mathrm{a/bd}y}^{\mathrm{o}} = \sum c_{\mathrm{i}}\left(\dot{y}_{\mathrm{c}} - \dot{y}_{\mathrm{a/be}j}\right) \tag{49}$$

where, c_{i} is the damping coefficient in roller-carrier contact; $Q_{\mathrm{a/bi}}$ is the inner/outer planetary bearing roller-carrier contact force; f_{bo} is the inner/outer planetary bearing roller-carrier friction force, which are given by

$$Q_{\mathrm{a/bi}} = \zeta_{\mathrm{a/bi}}K_{\mathrm{i}}\delta_{\mathrm{a/bi}}^{\frac{10}{9}} \tag{50}$$

$$f_{\mathrm{a/bi}} = \mu Q_{\mathrm{a/bi}} \tag{51}$$

where, $\zeta_{\mathrm{a/bi}}$ is the inner/outer planetary bearing roller-carrier contact factor, $\zeta_{\mathrm{a/bi}}$=1 when $\delta_{\mathrm{a/bi}}$>0, $\zeta_{\mathrm{a/bi}}$=0 when $\delta_{\mathrm{a/bi}}\leq$0; K_{i} is the contact stiffness between the roller and inner ring (carrier); $\delta_{\mathrm{a/bi}}$ is the inner/outer planetary bearing roller-carrier contact deformation, which is given by

$$\delta_{\mathrm{a/bi}} = \left(x_{\mathrm{c}} - x_{\mathrm{a/be}}\right)\cos\theta_{\mathrm{a/b}j} + \left(y_{\mathrm{c}} - y_{\mathrm{a/be}}\right)\sin\theta_{\mathrm{a/b}j} - 0.5C_{\mathrm{r}} \tag{52}$$

where C_{r} is the planetary bearing clearance.

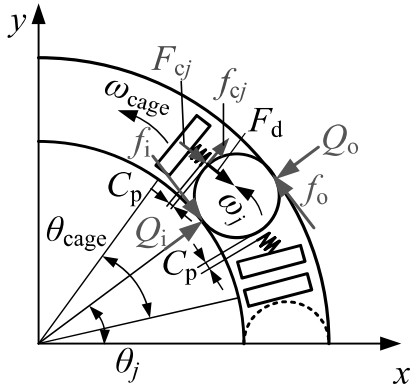

Fig. 4. Force analysis of rollers.

The roller force analysis is given in Fig. 4, the dynamic equations of planetary bearing roller are expressed as

$$\begin{aligned} &m_e\ddot{x}_{ej} = -Q_o(j)\cos\theta_j + Q_i(j)\cos\theta_j - c_o\left(\dot{x}_{ej} - \dot{x}_p\right) + c_i\left(\dot{x}_c - \dot{x}_{ej}\right) + F_{cj}\sin\theta_j \\ &-f_{cj}\sin\theta_j - f_{oj}\sin\theta_j + f_{ij}\sin\theta_j + F_{c1}\cos\phi_c + F_{c2}\cos\theta_j + F_d\sin\theta_j \end{aligned} \tag{53}$$

$$\begin{aligned} &m_e\ddot{y}_{cj} = -Q_o(j)\sin\theta_j + Q_i(j)\sin\theta_j - c_o\left(\dot{y}_{cj} - \dot{y}_p\right) + c_i\left(\dot{y}_c - \dot{y}_{cj}\right) - F_{cj}\cos\theta_j \\ &+f_{cj}\sin\theta_j + f_{oj}\cos\theta_j - f_{ij}\cos\theta_j + F_{c1}\sin\phi_c + F_{c2}\sin\theta_j - F_d\cos\theta_j \end{aligned} \tag{54}$$

$$I_e\ddot{\phi}_{cj} = \left(F_f^o + F_f^i - f_{cj}\right)\frac{D_w}{2} \tag{55}$$

$$I_{ec}\ddot{\theta}_{cj} = F_f^o R_o - F_f^i R_i - F_{cj}\frac{d_m}{2} - F_d\frac{d_m}{2} \tag{56}$$

where, m_e is the planetary bearing roller mass; I_e is the planetary bearing roller moment of inertia around roller axis; I_{ec} is the planetary bearing roller moment of inertia about the planetary bearing axis; x_e and y_e are the roller displacements; ϕ_e and θ_e are the roller angular displacements around its axis and planetary bearing axis; F_{c1} and F_{c2} are the centrifugal forces rotating about the planetary bearing axis and planetary gear set axis as given in Fig. 5. The calculation method is given by

$$F_{c1} = m_e\dot{\theta}_c^2\overline{oo_r} \tag{57}$$

$$F_{c2} = m_e\dot{\theta}_{cj}^2\frac{d_m}{2} \tag{58}$$

where, $\overline{oo_r}$ is the planetary gear set-roller center distance, which is given by

$$\overline{oo_r} = \sqrt{\left(\frac{d_m}{2}\sin\theta_{ej} + \frac{m\left(Z_s + Z_p\right)}{2}\sin\varphi_p\right)^2 + \left(\frac{d_m}{2}\cos\theta_{ej} + \frac{m\left(Z_s + Z_p\right)}{2}\cos\varphi_p\right)^2} \tag{59}$$

$$\varphi_c = \arctan\left(\frac{d_m\cos\theta_{ej} + m\left(Z_s + Z_p\right)\cos\varphi_p}{d_m\sin\theta_{ej} + m\left(Z_s + Z_p\right)\sin\varphi_p}\right) \tag{60}$$

$$\varphi_p = \theta_c + \frac{2(n-1)\pi}{n} \tag{61}$$

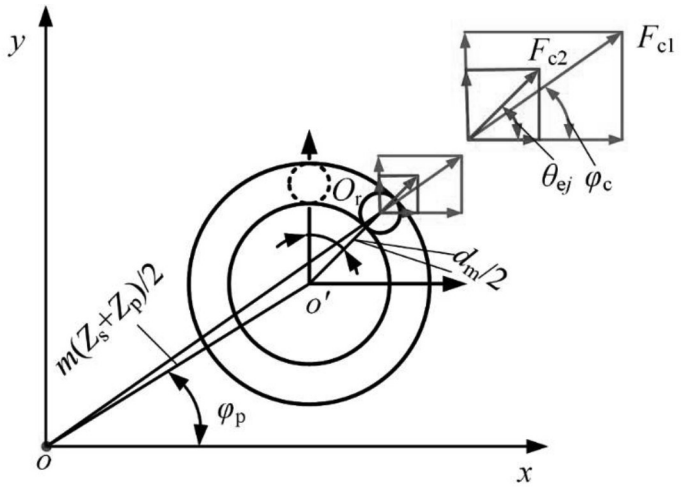

Fig. 5. Roller centrifugal forces.

The dynamic equations of planetary bearing cage are expressed as

$$m_g\ddot{x}_g = -F_{cj}\sin\theta_j - f_{cj}\cos\theta_j + F_{cx} \tag{62}$$

$$m_g\ddot{y}_g = F_{cj}\cos\theta_j - f_{cj}\sin\theta_j + F_{cy} - G \tag{63}$$

$$I_g\ddot{\theta}_g = M_{cage} + F_{cj}\frac{d_m}{2} \tag{64}$$

where, m_g is the cage mass; I_g is the cage moment of inertia around its own axis; x_g and y_g are the cage displacements; θ_g is the angular displacement around its axis; G is the cage gravity; F_{cj} is the roller-cage impact force; f_{cj} is the roller- cage friction force, which are given by

$$\begin{cases} F_{cj} = K_{cage}\left[\left(\theta_j - \theta_{cage}\right)\dfrac{d_m}{2} - C_p\right] & \left(\theta_j - \theta_{cage}\right) > 0 \\ F_{cj} = K_{cage}\left[\left(\theta_j - \theta_{cage}\right)\dfrac{d_m}{2} + C_p\right] & \left(\theta_j - \theta_{cage}\right) < 0 \end{cases} \tag{65}$$

$$f_{cj} = \mu F_{cj} \tag{66}$$

where, K_{cage} is the pocket contact stiffness between the roller and cage, and C_p is the cage pocket clearance.

4. Results and discussion

In this section, a DPGS is used to analyze the vibrations of planetary bearing. The gear parameters of DPGS are shown in Table 1. The planetary bearing parameters of DPGS are shown in Table 2. The carrier rotation speed is 400r/min in the following analysis.

Table 1. Gear parameters of DPGS.

	Sun gear	Ring gear	Inner planet	Outer planet	Carrier
Teeth number	34	82	21	22	-
Module (mm)	4	4	4	4	-
Pressure angle (°)	25	25	25	25	-
Face width (mm)	38	38	38	8	-
Mass (kg)	2.27	7.008	1.196	1.36	7.008
Bearing stiffness (N/m)	1×10^8	1×10^8	-	-	1×10^8

Table 2. Planetary bearing parameters of DPGS.

Parameters	Value	Parameters	Value
Roller number	22	Roller length(mm)	28.5
Inner ring diameter(mm)	38	Clearance(μm)	10

Outer ring diameter(mm)	46	Pocket clearance(μm)	20
Roller diameter(mm)	4	Cage guidance clearance(mm)	0.52

4.1 Effect of the sun gear rotation speed on the planetary bearing contact force

The dynamic model is solved by the fourth-order Runge-Kutta method. The initial displacements are 10^{-6} m. The initial velocities are 0 m/s. The initial angular displacements are 0 rad. The initial roller angular velocities around its axis are set to 0.9 times of that in the case of pure rolling. The other angular velocities are set to the values in the case of pure rolling.

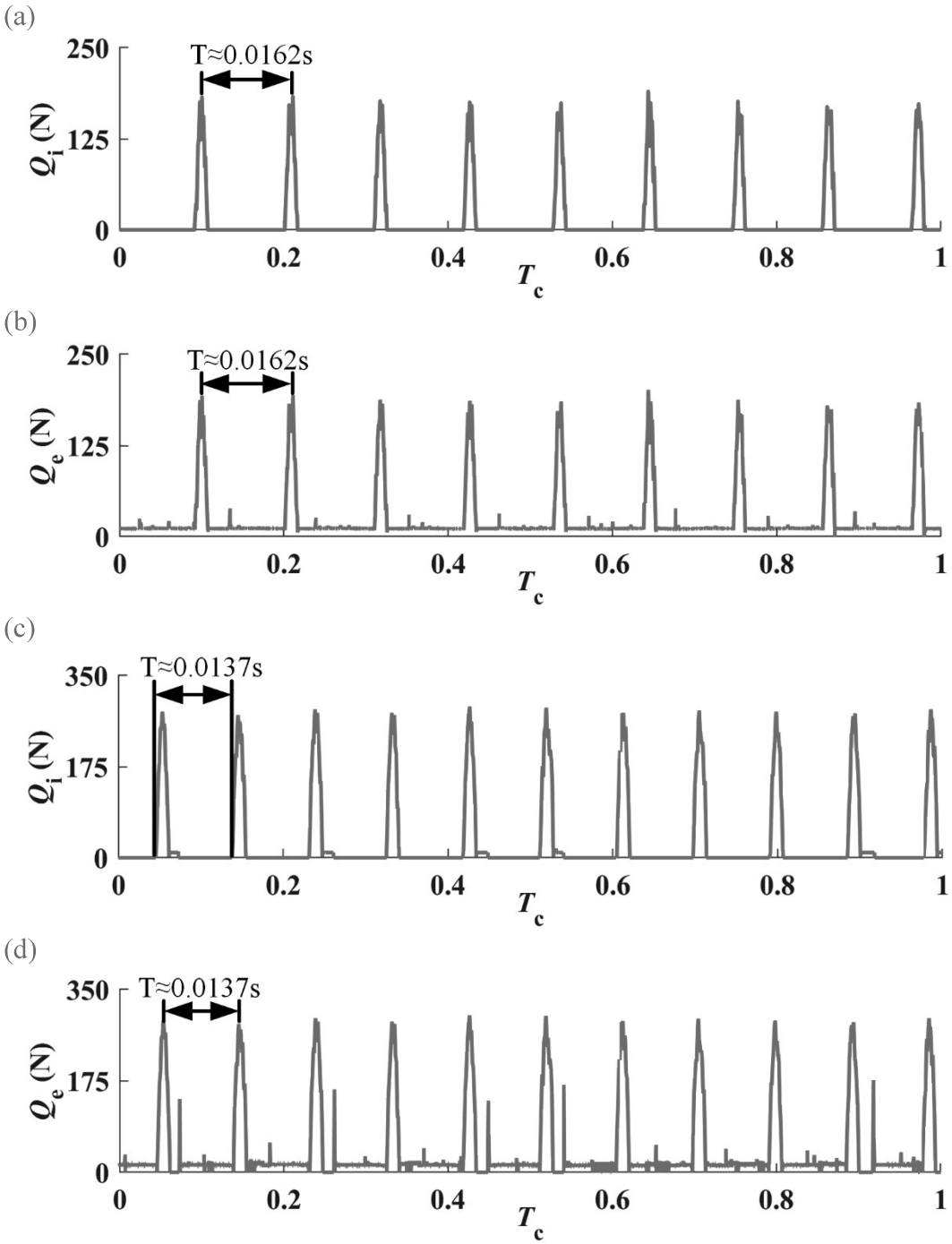

Fig. 6. (a) The inner ring-roller contact force of inner planetary bearing; (b) the outer ring-roller contact force of inner planetary bearing; (c) the inner ring-roller contact force of outer planetary bearing contact force; and (d) the outer ring-roller contact force of outer planetary bearing contact force.

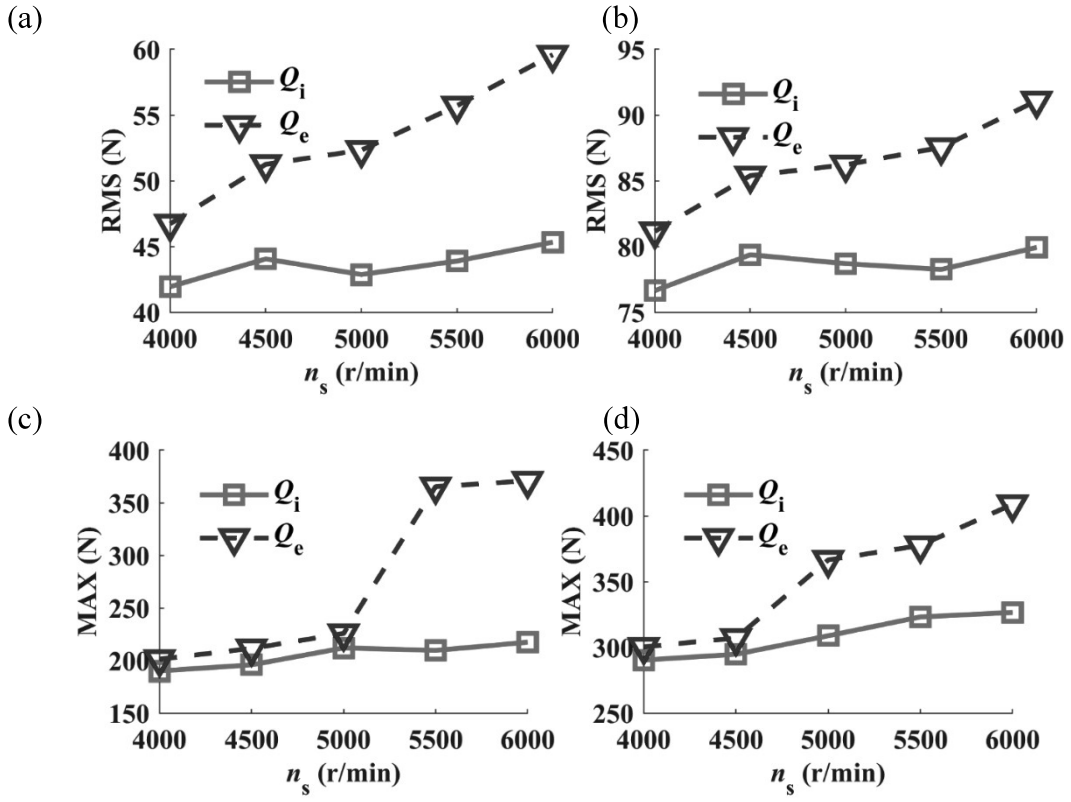

Fig. 7. Effect of the sun gear rotation speed on the (a) RMS value of inner planetary bearing contact force; (b) RMS value of inner planetary bearing contact force; (c) MAX value of outer planetary bearing contact force; and (d) MAX value of outer planetary bearing contact force.

Fig. 6 gives the time-domain planetary bearing contact force when the sun gear rotation speed is 4000rpm. The inner/outer planetary bearing contact force exhibit obvious periodic variations. The period of inner planetary bearing contact force is about 0.0162s and that of outer planetary bearing contact force has a period of 0.0137s. Thus, the periodic frequency of inner planetary bearing contact force is about 61.73Hz and that of outer planetary bearing contact force is about 71.72Hz. The inner planetary bearing cage rotation period is 0.0146s without the roller slip; and the outer planetary bearing cage rotation period is 0.0153s without the roller slip. Thus, the periodic frequency of inner planetary bearing cage rotation period (f_{ga}) is about 68.49Hz; and that of outer planetary bearing cage rotation period (f_{gb}) is about 65.36Hz. The carrier rotation periodic frequency (f_c) is about 6.67 Hz. The contact force periodic frequency of inner planetary bearing approximately equal to f_{ga}-f_c; and that of outer planetary bearing approximately equal to f_{ga}+f_c. This is because the inner planetary bearing cage and the carrier rotate in the same direction, while the outer planetary bearing cage and carrier rotate in the opposite direction. The effect of the sun gear rotation speed on the planetary bearing contact force is given in Fig. 7. In Fig. 7, the inner/outer planetary bearing contact force root mean square (RMS) and maximum (MAX) values of different sun gear rotation speeds are given. The RMS and MAX values of inner/outer planetary bearing contact force generally increase with the increment of sun gear rotation speed. Figure 7(a) illustrates the effect of the sun gear rotation speed on the RMS value of inner planetary bearing contact force. When the sun gear rotation speed is from 4000rpm to 6000rpm, the RMS value of inner planetary bearing inner ring-roller contact force is from 41.95N to 45.33N; and the RMS value of inner planetary bearing outer ring-roller contact force is from 46.73N to 59.59N. Figure 7(b) illustrates the effect of the sun gear rotation speed on the RMS value of outer planetary bearing contact force. When the sun gear rotation speed is from 4000rpm to 6000rpm, the RMS value of outer planetary bearing

inner ring-roller contact force is from 76.65N to 79.93N, and the RMS value of outer planetary bearing outer ring-roller contact force is from 81.16N to 91.08N. Figure 7(c) illustrates the effect of the sun gear rotation speed on the MAX value of inner planetary bearing contact force. When the sun gear rotation speed is from 4000rpm to 6000rpm, the MAX value of inner planetary bearing inner ring-roller contact force is from 190.13N to 217.42N; and the MAX value of inner planetary bearing outer ring-roller contact force is from 201.33N to 370.85N. Figure 7(d) illustrates the effect of the sun gear rotation speed on the MAX value of outer planetary bearing contact force. When the sun gear rotation speed is from 4000rpm to 6000rpm, the MAX value of outer planetary bearing inner ring-roller contact force is from 290.36N to 326.59N, and the MAX value of outer planetary bearing outer ring-roller contact force is from 300.42N to 408.8N.

4.2 Effect of the sun gear rotation speed on the planetary bearing roller-cage impact force

Fig. 8 gives the time-domain planetary bearing roller-cage impact force when the sun gear rotation speed is 4000rpm. The inner/outer planetary bearing roller-cage impact force exhibit obvious periodic variations. The effect of the sun gear rotation speed on the planetary bearing roller-cage impact force is given in Fig. 9. In Fig. 9, the RMS and MAX values of planetary bearing roller-cage impact force for different sun gear rotation speeds are given. The RMS and MAX values of inner/outer planetary bearing roller-cage impact force generally increase with the increment of sun gear rotation speed. Fig. 9(a) illustrates the effect of the sun gear rotation speed on the RMS value of inner planetary bearing roller-cage impact force. When the sun gear rotation speed is from 4000rpm to 6000rpm, the RMS value of inner planetary bearing roller-cage impact force is from 1.82N to 2.86N. Fig. 9(b) illustrates the effect of the sun gear rotation speed on the RMS value of outer planetary bearing roller-cage impact force. When the sun gear rotation speed is from 4000rpm to 6000rpm, the RMS value of outer planetary bearing roller-cage impact force is from 1.39N to 2.97N. Fig. 9(c) illustrates the effect of the sun gear rotation speed on the MAX value of inner planetary bearing roller-cage impact force. When the sun gear rotation speed is from 4000rpm to 6000rpm, the MAX value of inner planetary bearing roller-cage impact force is from 61.89N to 98.02N. Fig. 9(d) illustrates the effect of the sun gear rotation speed on the MAX value of outer planetary bearing roller-cage impact force. When the sun gear rotation speed is from 4000rpm to 6000rpm, the MAX value of outer planetary bearing roller-cage impact force is from 56.9N to 88.45N.

(a)

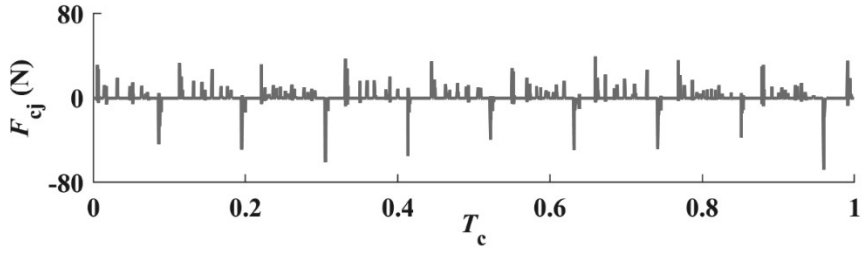

(b)

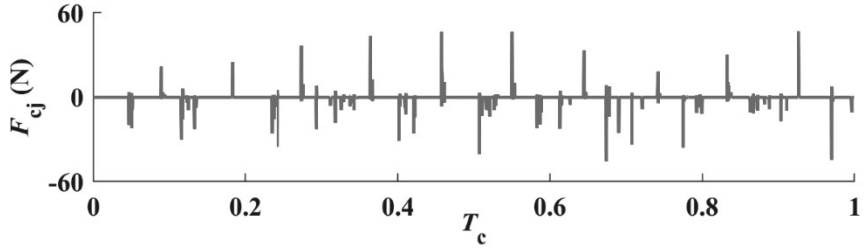

Fig. 8. Time-domain (a) inner planetary bearing roller-cage impact force; and (b) outer planetary bearing roller-cage impact force.

(a) (b)

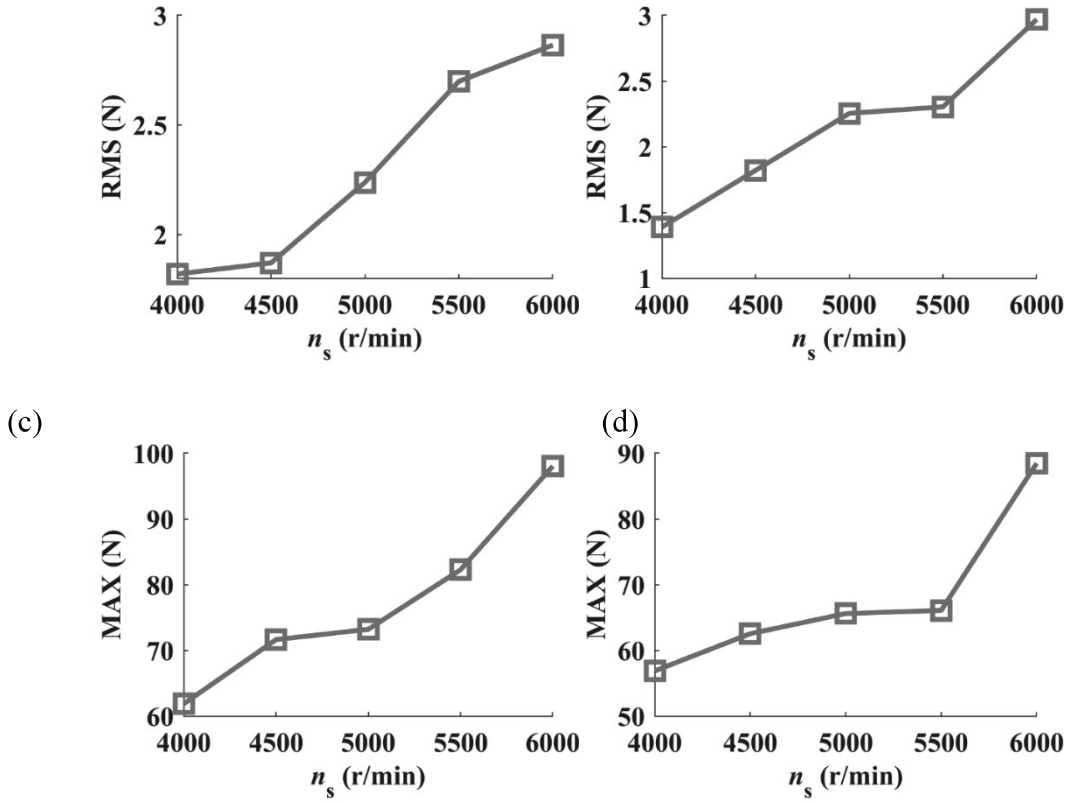

Fig. 9. Effect of the sun gear rotation speed on the (a) RMS value of inner planetary bearing roller-cage impact force; (b) RMS value of inner planetary bearing roller-cage impact force; (c) MAX value of outer planetary bearing roller-cage impact force; and (d) MAX value of outer planetary bearing roller-cage impact force.

4.2 Effect of the sun gear rotation speed on the planetary bearing vibrations

Fig. 10 gives the time-domain planetary bearing roller acceleration when the sun gear rotation speed is 4000rpm. The inner/outer planetary bearing roller acceleration exhibit obvious periodic variations. The effect of the sun gear rotation speed on the planetary bearing roller acceleration is shown in Fig. 11. In Fig. 11, the RMS and MAX values of inner/outer planetary bearing roller acceleration for different sun gear rotation speeds are given. The RMS and MAX values of inner/outer planetary bearing roller acceleration generally increase with the increment of sun gear rotation speed. Fig. 11(a) illustrates the effect of the sun gear rotation speed on the RMS value of inner planetary bearing roller acceleration. When the sun gear rotation speed is from 4000rpm to 6000rpm, the RMS value of inner planetary bearing roller acceleration in x direction is from 1970.53m/s^2 to 3253.35m/s^2; and the RMS value of inner planetary bearing roller acceleration in y direction is from 2012.65m/s^2 to 3203.17m/s^2. Fig. 11(b) illustrates the effect of the sun gear rotation speed on the RMS value of outer planetary bearing roller acceleration. When the sun gear rotation speed is from 4000rpm to 6000rpm, the RMS value of outer planetary bearing roller acceleration in x direction is from 3978.8m/s^2 to 4407.24m/s^2; and the RMS value of outer planetary bearing roller acceleration in y direction is from 3953.7m/s^2 to 4716.4m/s^2. Fig. 11(c) illustrates the effect of the sun gear rotation speed on the MAX value of inner planetary bearing roller acceleration. When the sun gear rotation speed is from 4000rpm to 6000rpm, the MAX value of inner planetary bearing roller acceleration in x direction is from 1.416×10^4m/s^2 to 1.231×10^5m/s^2; and the MAX value of inner planetary bearing roller acceleration in y direction is from 1.285×10^4m/s^2 to 1.05×10^5m/s^2. Fig. 11(d) illustrates the effect of the sun gear rotation speed on the MAX value of outer planetary bearing roller acceleration. When the sun gear rotation speed is from 4000rpm to 6000rpm, the MAX

value of outer planetary bearing roller acceleration in x direction is from 4.489×10^4m/s^2 to 1.179×10^5m/s^2; and the MAX value of outer planetary bearing roller acceleration in y direction is from 5.779×10^4m/s^2 to 1.176×10^5m/s^2.

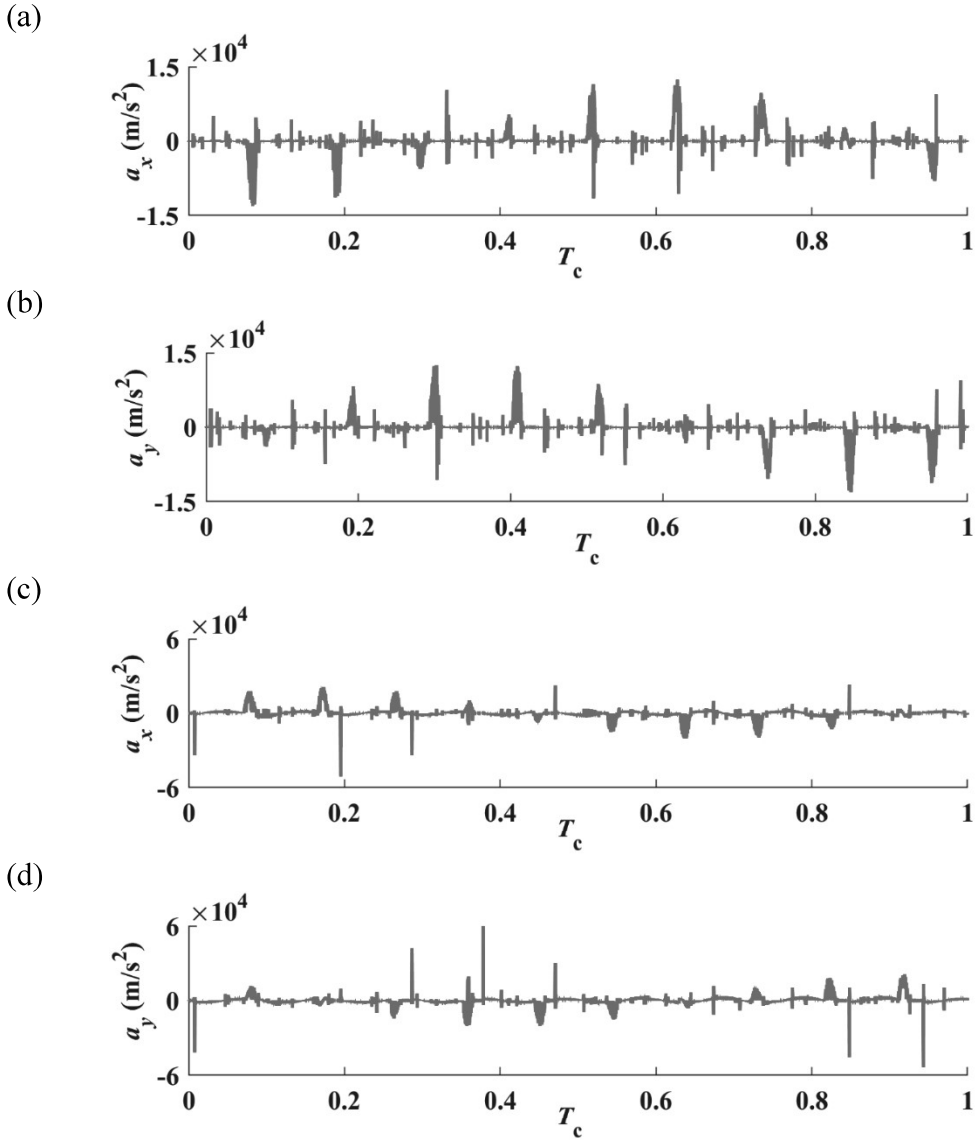

Fig. 10. Time-domain (a) inner planetary bearing roller vibrations in x direction; (b) inner planetary bearing roller vibrations in y direction; (c) outer planetary bearing roller vibrations in x direction; and (d) outer planetary bearing roller vibrations in y direction.

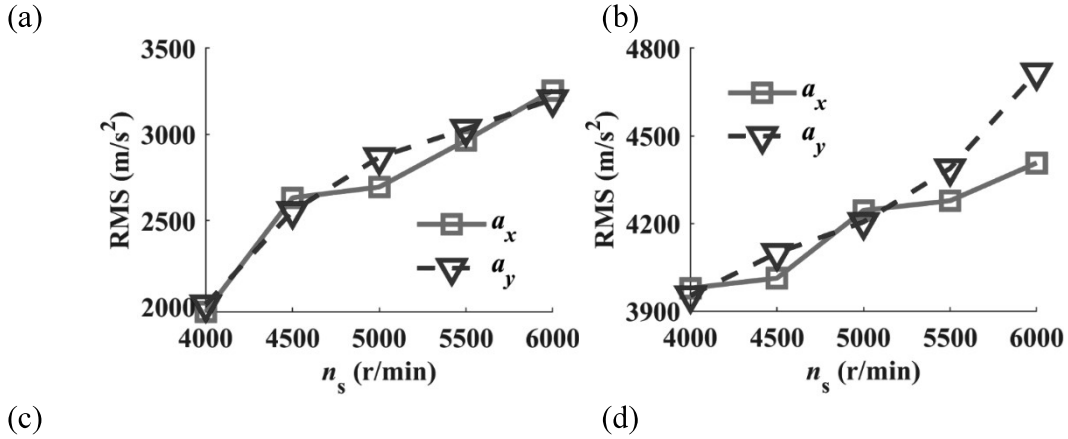

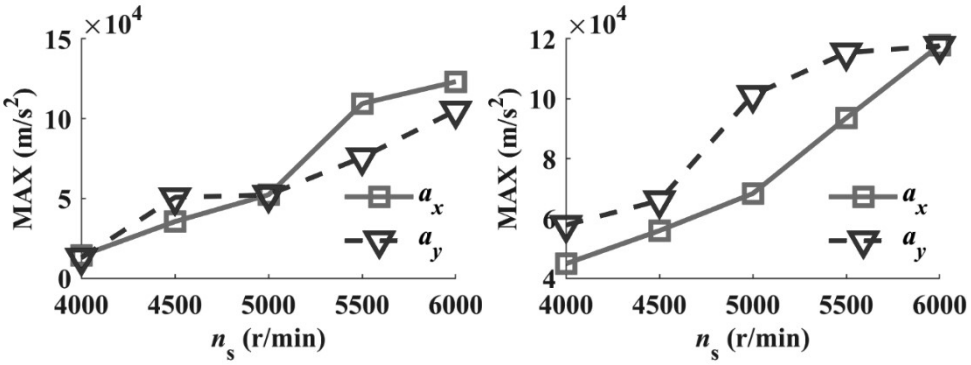

Fig. 11. Effect of the sun gear rotation speed on the (a) RMS value of inner planetary bearing roller; (b) RMS value of outer planetary bearing roller; (c) MAX value of inner planetary bearing roller; and (d) MAX value of outer planetary bearing roller.

(a)

(b)

(c)

(d)

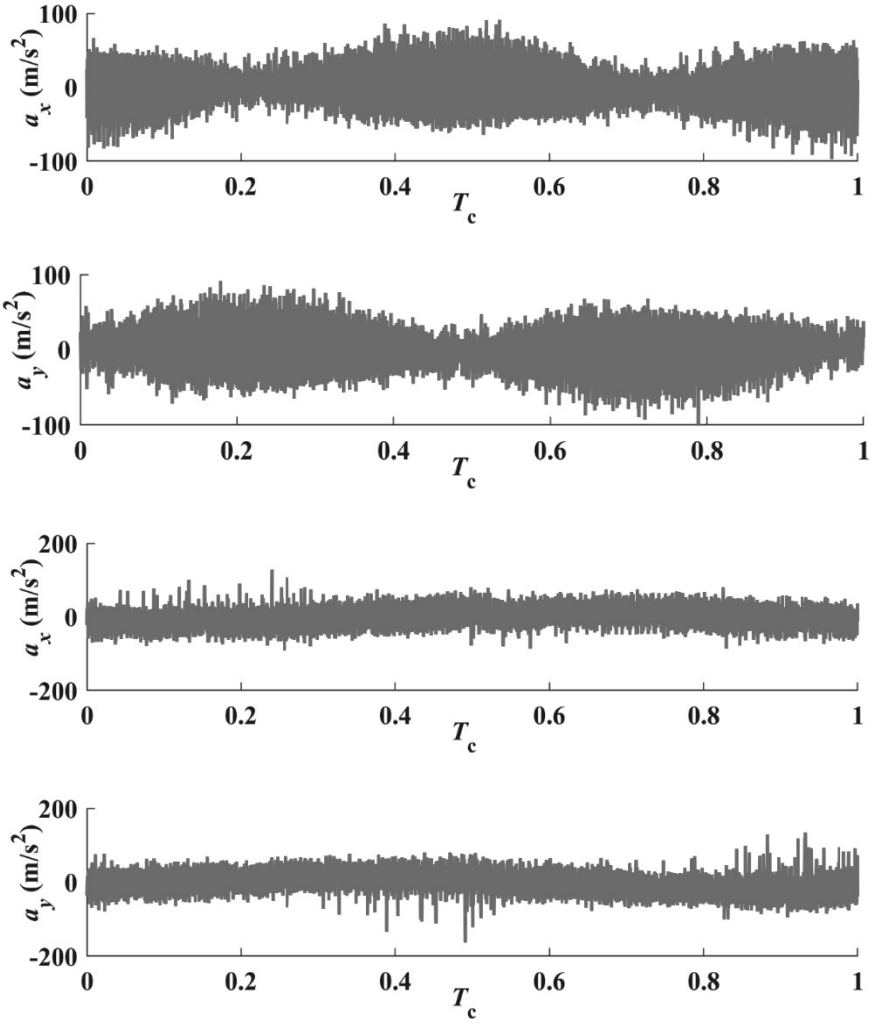

Fig. 12. Time-domain (a) inner planet vibrations in *x* direction; (b) inner planet vibrations in *y* direction; (c) outer planet vibrations in *x* direction; and (d) outer planet vibrations in *y* direction.

Fig. 12 gives the time-domain planet acceleration when the sun gear rotation speed is 4000rpm. The inner/outer planet acceleration exhibit obvious periodic variations. The effect of sun gear rotation speed on the planet acceleration is given in Fig. 13. In Fig. 13, the RMS and MAX values of inner/outer planet acceleration for different sun gear rotation speeds are given. The RMS and MAX values of inner/outer planet acceleration generally increase with the increment of sun gear rotation speed. Fig. 13(a) illustrates the effect of the sun gear rotation

speed on the RMS value of inner planet acceleration. When the sun gear rotation speed is from 4000rpm to 6000rpm, the RMS value of inner planet acceleration in x direction is from 25.73m/s^2 to 43.82m/s^2; and the RMS value of inner planet acceleration in y direction is from 25.57m/s^2 to 43.88m/s^2. Fig. 13(b) illustrates the effect of the sun gear rotation speed on the RMS value of outer planet acceleration. When the sun gear rotation speed is from 4000rpm to 6000rpm, the RMS value of outer planet acceleration in x direction is from 24.99m/s^2 to 42.21m/s^2; and the RMS value of outer planet acceleration in y direction is from 26.55m/s^2 to 42.86m/s^2. Fig. 13(c) illustrates the effect of sun gear rotation speed on the MAX value of inner planet acceleration. When the sun gear rotation speed is from 4000rpm to 6000rpm, the inner planet acceleration MAX value in x direction is from 97.04m/s^2 to 243.53m/s^2; and the MAX value of inner planet acceleration in y direction is from 104.23m/s^2 to 283.67m/s^2. Fig. 13(d) illustrates the effect of the sun gear rotation speed on the MAX value of outer planet acceleration. When the sun gear rotation speed is from 4000rpm to 6000rpm, the MAX value of outer planet acceleration in x direction is from 128.24m/s^2 to 316.15m/s^2; and the MAX value of outer planet acceleration in y direction is from 162.69m/s^2 to 354.89m/s^2.

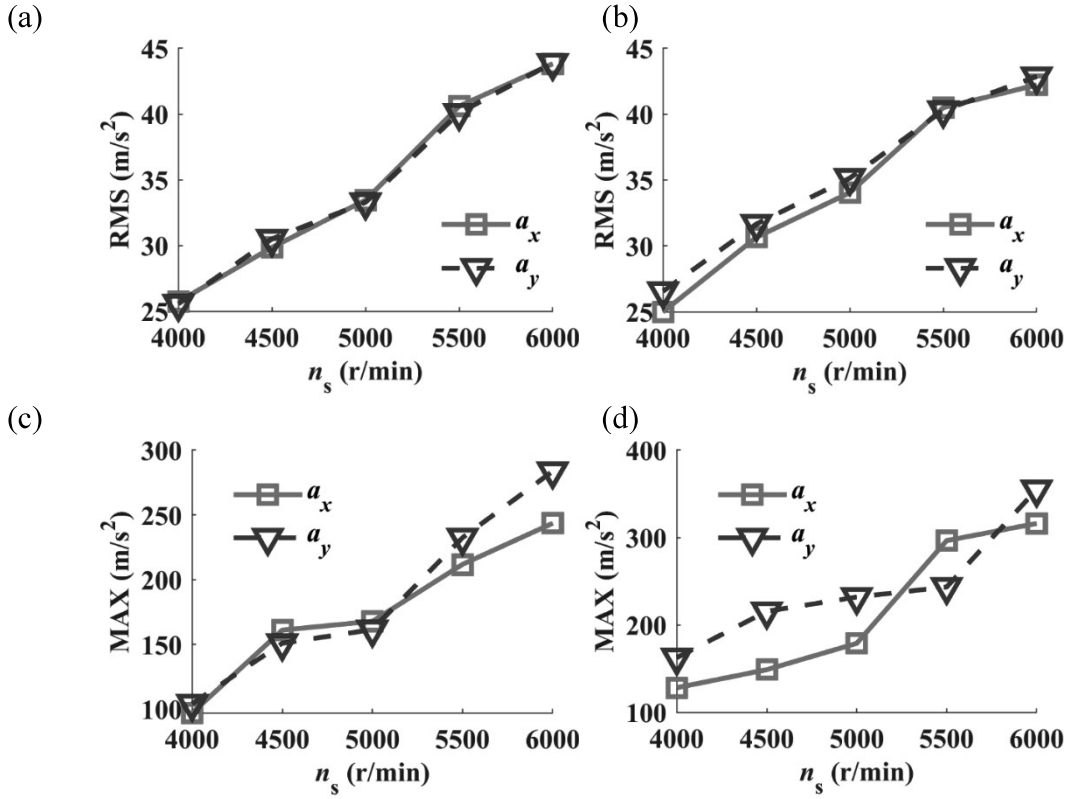

Fig. 13. Effect of the sun gear rotation speed on the (a) RMS value of inner planet; (b) RMS value of outer planet; (c) MAX value of inner planet; and (d) MAX value of outer planet.

Fig. 14 gives the time-domain carrier acceleration when the sun gear rotation speed is 4000rpm. The effect of the sun gear rotation speed on the planet acceleration is given in Fig. 15. In Fig. 15, the RMS and MAX values of carrier acceleration for different sun gear rotation speeds are given. The RMS and MAX values of carrier acceleration generally increase with the increment of sun gear rotation speed. Fig. 15(a) illustrates the effect of the sun gear rotation speed on the RMS value of carrier acceleration. When the sun gear rotation speed is from 4000rpm to 6000rpm, the RMS value of inner planet acceleration in x direction is from 4.02m/s^2 to 7.08m/s^2; and the RMS value of inner planet acceleration in y direction is from 4.12m/s^2 to 7.14m/s^2. Fig. 15(b) illustrates the effect of the sun gear rotation speed on the MAX value of carrier acceleration. When the sun gear rotation speed is from 4000rpm to 6000rpm, the MAX

value of carrier acceleration in x direction is from 13.56m/s^2 to 27.71m/s^2; and the MAX value of carrier acceleration in y direction is from 15.12m/s^2 to 27.22m/s^2.

(a)

(b)

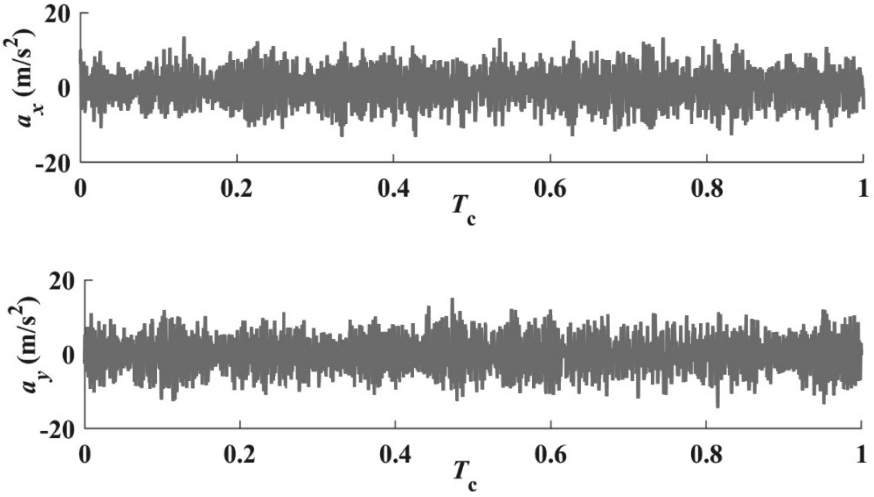

Fig. 14. Time-domain vibrations of carrier in (a) x and (b) y directions.

(a) (b)

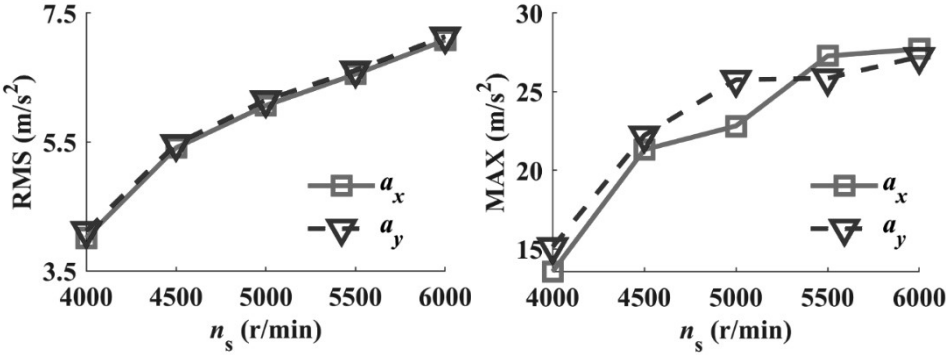

Fig. 15. Effect of the sun gear rotation speed on the (a) RMS and (b) MAX values of carrier accelerations.

(a)

(b)

(c)

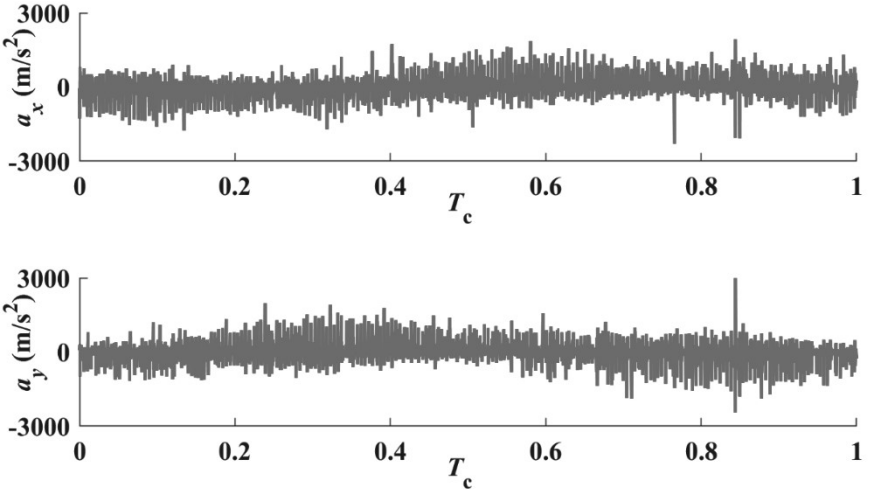

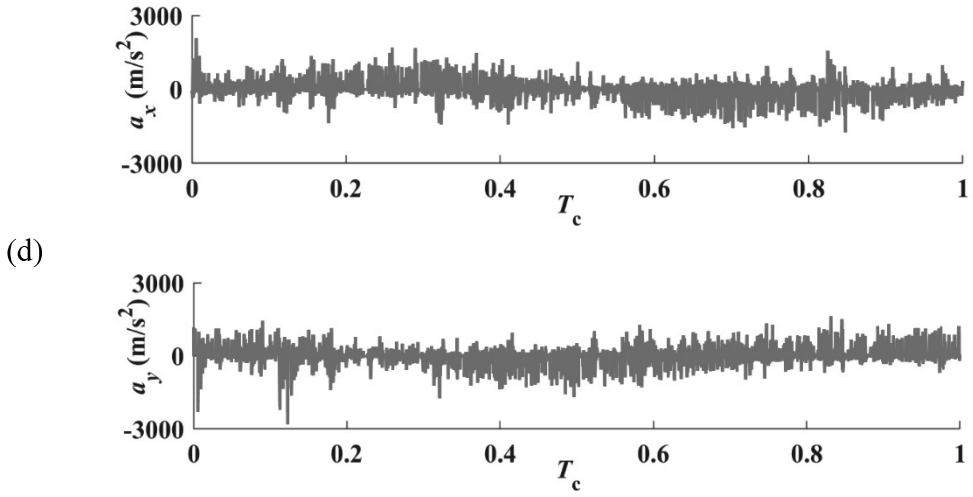

Fig. 16. Time-domain accelerations of the (a) inner planetary bearing cage in *x* direction; (b) inner planetary bearing cage in *y* direction; (c) outer planetary bearing cage in *x* direction; and (d) outer planetary bearing cage in *y* direction.

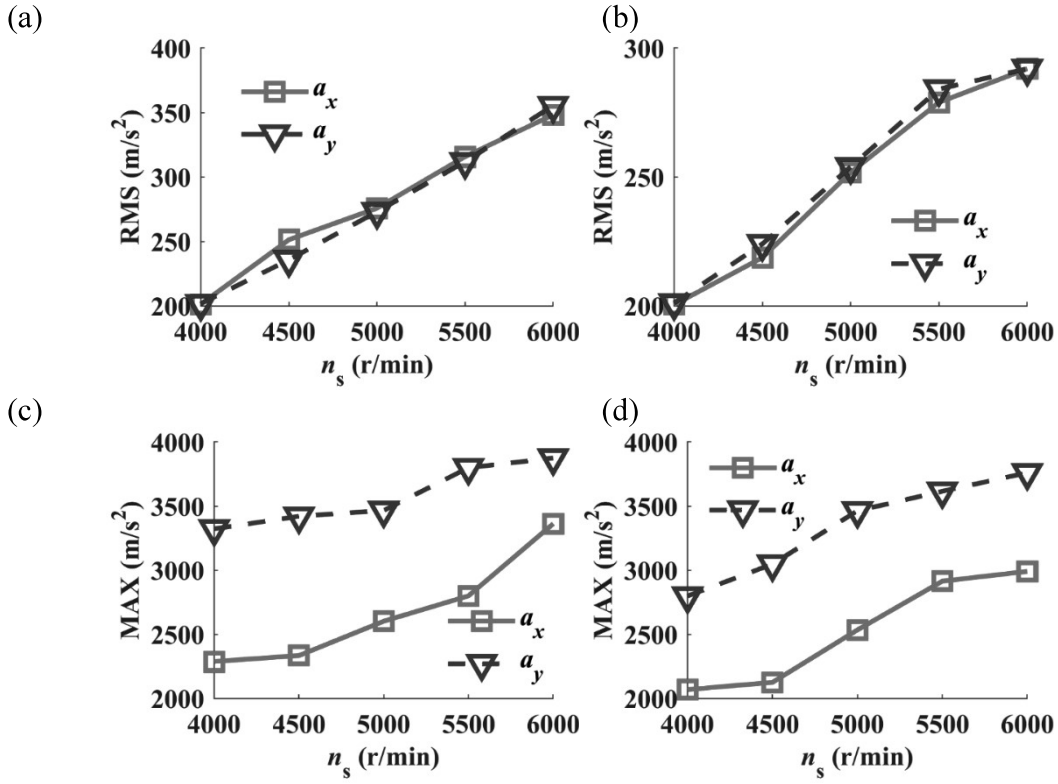

Fig. 17. Effect of the sun gear rotation speed on the (a) RMS value of inner planetary bearing cage; (b) RMS value of outer planetary bearing cage; (c) MAX value of inner planetary bearing cage; and (d) MAX value of outer planetary bearing cage.

Fig. 16 gives the time-domain planetary bearing cage acceleration when the sun gear rotation speed is 4000rpm. The inner/outer planetary bearing cage acceleration exhibit obvious periodic variations. The effect of the sun gear rotation speed on the planetary bearing cage acceleration is given in Fig. 17. In Fig. 17, the RMS and MAX values of inner/outer planetary bearing cage acceleration for different sun gear rotation speeds are given. The RMS and MAX values of inner/outer planetary bearing cage acceleration generally increase with the increment of sun gear rotation speed. Fig. 17(a) illustrates the effect of the sun gear rotation speed on the RMS value of inner planetary bearing cage acceleration. When the sun gear rotation speed is

from 4000rpm to 6000rpm, the RMS value of inner planetary bearing cage acceleration in x direction is from 201.3m/s^2 to 348.2m/s^2; and the RMS value of inner planetary bearing cage acceleration in y direction is from 201.8m/s^2 to 355.4m/s^2. Fig. 17(b) illustrates the effect of the sun gear rotation speed on the RMS value of outer planetary bearing cage acceleration. When the sun gear rotation speed is from 4000rpm to 6000rpm, the RMS value of outer planetary bearing cage acceleration in x direction is from 200.5m/s^2 to 291.9m/s^2; and the RMS value of outer planetary bearing cage acceleration in y direction is from 201.1m/s^2 to 292m/s^2. Fig. 17(c) illustrates the effect of the sun gear rotation speed on the MAX value of inner planetary bearing cage acceleration. When the sun gear rotation speed is from 4000rpm to 6000rpm, the MAX value of inner planetary bearing cage acceleration in x direction is from 2287.7m/s^2 to 3361.9m/s^2; and the MAX value of inner planetary bearing cage acceleration in y direction is from 3322.4m/s^2 to 3874.2m/s^2. Fig. 17(d) illustrates the effect of the sun gear rotation speed on the MAX value of outer planetary bearing cage acceleration. When the sun gear rotation speed is from 4000rpm to 6000rpm, the MAX value of outer planetary bearing cage acceleration in x direction is increased 2068.8m/s^2 to 2990.5m/s^2; and the MAX value of outer planetary bearing cage acceleration in y direction is from 2798.1m/s^2 to 3759.4m/s^2.

4.3 Experimental verification and comparison

The DPGS vibration test rig is plotted in Fig. 18. Two servo motors are included in the test ring. One motor is used to adjust the carrier rotation speed. The other one is used to adjust the sun gear rotation speed. The servo motors are controlled by the control cubicle. The rotation speed and torque signal will be transmitted to the data acquisition system. Moreover, the DPGS vibrations are collected by a triaxial acceleration sensor installed on the carrier bearing housing and near the carrier axis. The acceleration signals from experiment and simulation are compared to prove the correctness of proposed model. The acceleration signals are obtained when the sun gear rotation speed is 4000rpm. The simulated acceleration signals are the acceleration of each part in the DPGS in the cartesian coordinate system. However, the triaxial acceleration sensor installed on the carrier bearing housing and near the carrier axial. The experimental acceleration signals are not the acceleration of any part in the DPGS. Thus, the simulated acceleration signals cannot be directly compared with the experimental ones. Considering the transmission path effect, the simulated acceleration signals can be given by [28]

$$a_{\mathrm{p}}(t)=C_{\mathrm{s}}a_{\mathrm{s}}(t)+C_{\mathrm{c}}a_{\mathrm{c}}(t)+C_{\mathrm{r}}a_{\mathrm{r}}(t)+\sum_{i=1}^{Z}\left(C_{\mathrm{a}}a_{\mathrm{a}}(t)+C_{\mathrm{b}}a_{\mathrm{b}}(t)\right) \tag{67}$$

where, C_{s}, C_{c}, C_{r}, C_{a}, and C_{b} are the sun gear, carrier, ring gear, inner planet, and outer planet vibration contribution coefficient, respectively (C_{s}=0.57, C_{c}=0.14, C_{r}=0.269, C_{a}=0.06(1-cos(θ_{t})), and C_{b}=0.06 in this work), detailed calculation method is given in Appendix A; a_{s}, a_{c}, a_{r}, a_{a}, and a_{b} are the acceleration signals of sun gear, carrier, ring gear, inner planet, and outer planet, respectively.

(a)

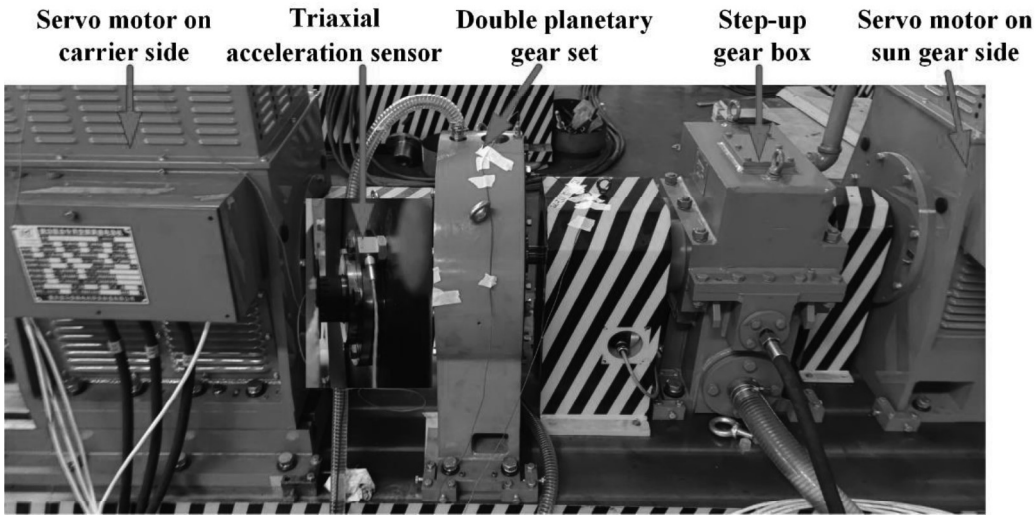

(b)

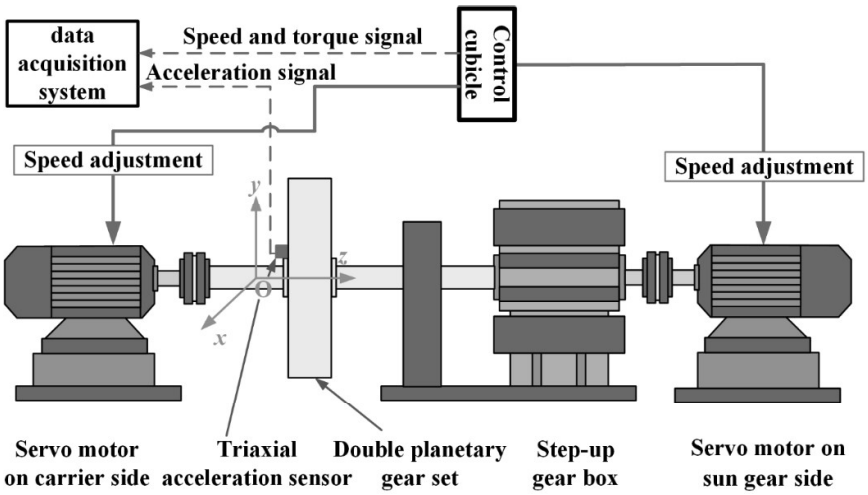

Fig. 18. A vibration test rig for DPGS. (a) Photograph and (b) Schematic diagram of test rig.

(a)

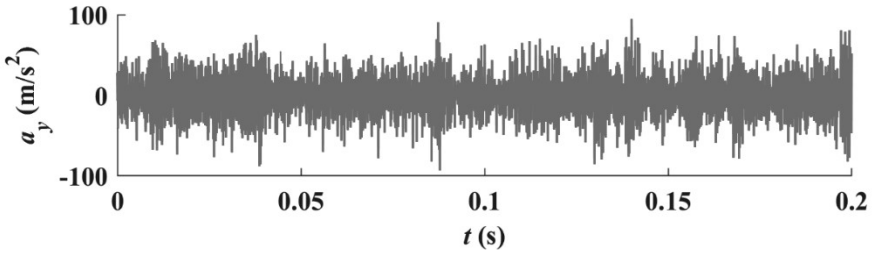

(b)

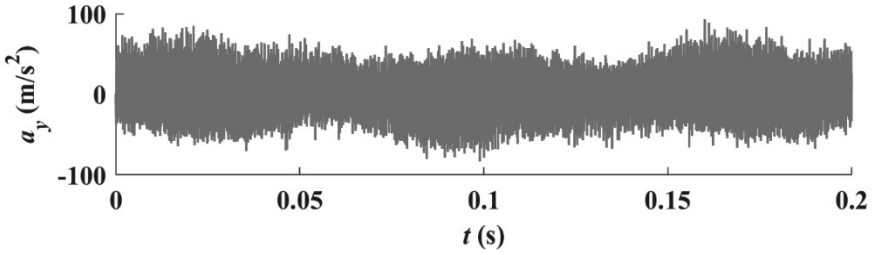

Fig. 19. Time-domain (a) experimental and (b) simulated acceleration signals of DPGS.

Fig. 19 gives the time-domain acceleration signals of DPGS. The experimental time-domain acceleration signals are shown in Fig. 19(a). In Fig. 19(a), the RMS value of experimental acceleration is 26.31m/s^2; and the MAX value of experimental acceleration is 94.44 m/s^2. The

simulated time-domain acceleration signals are shown in Fig. 19(b). In Fig. 19(b), the RMS value of simulated acceleration is 22.49m/s^2; and the MAX value of experimental acceleration is 93.42m/s^2. The difference of RMS values between the experimental and simulated accelerations is 14.54%. The difference of MAX values between the experimental and simulated accelerations is 1.1%.

(a)

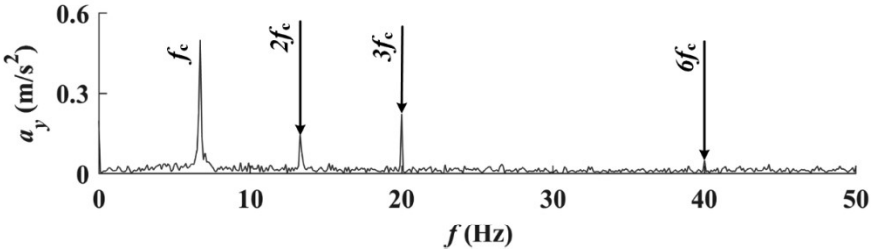

(b)

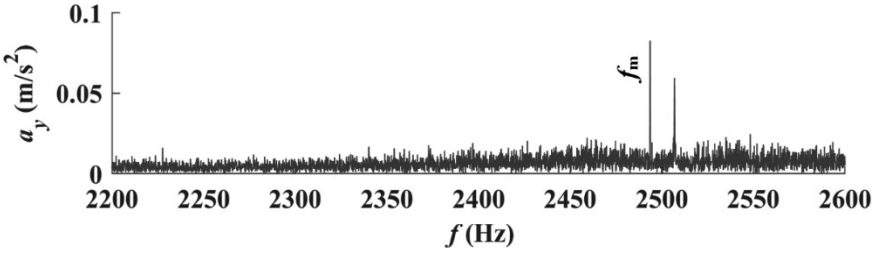

(c)

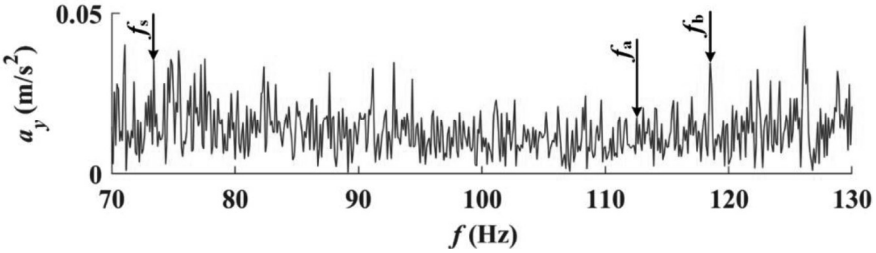

Fig. 20. Spectra of simulated DPGS acceleration signals. (a) 0-50Hz (b) 2200-2600Hz; and (c) 70-130Hz.

(a)

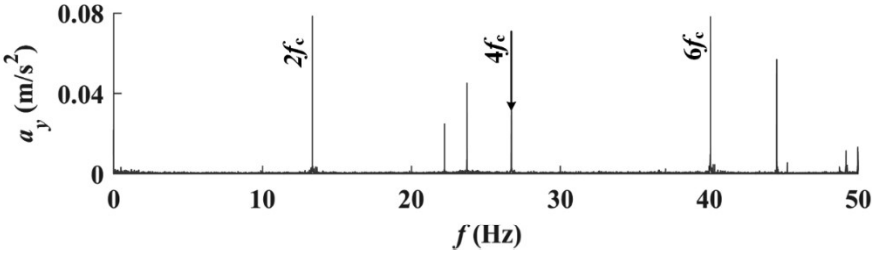

(b)

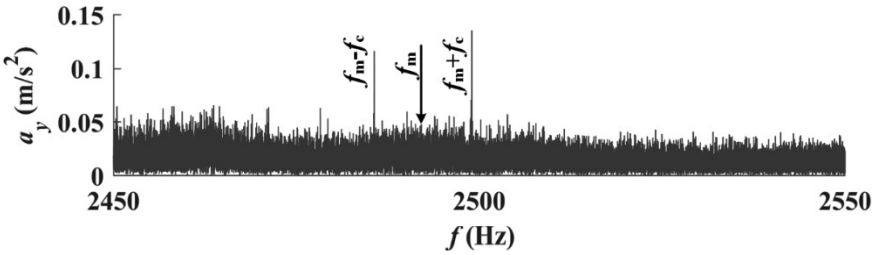

(c)

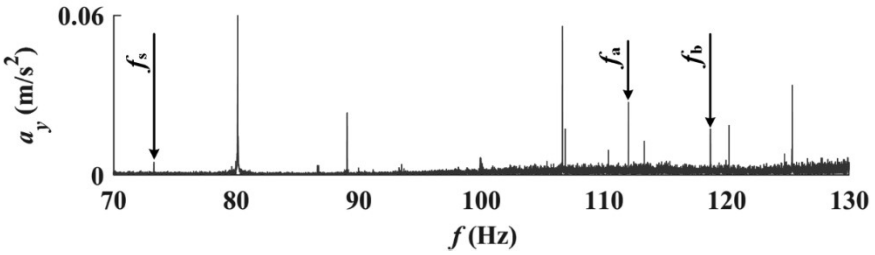

Fig. 21. Spectra of experimental DPGS acceleration signals. (a) 0-50Hz (b) 2200-2600Hz; and (c) 70-130Hz.

The spectra of simulated DPGS acceleration signals are given in Fig. 20. The spectra of experimental DPGS acceleration signals are given in Fig. 21. In Fig. 20 and Fig. 21, f_c, f_m, f_s, f_a, and f_b are the carrier rotation frequency, gear meshing frequency, sun gear rotation frequency, inner planet rotation frequency, and outer planet rotation frequency, respectively. The carrier rotation frequency in the simulated acceleration spectrum is 6.70Hz, while its experimental value is 6.68Hz. The gear meshing frequency in the simulated acceleration spectrum is 2493.64Hz, while its experimental value is 2493.20Hz. Besides, because the test rig has planet axis error, the amplitudes are obviously larger in $f_m \pm f_c$. The sun gear rotation frequency in the simulated acceleration spectrum is 73.41Hz, while its experimental value is 73.35Hz. The inner planet rotation frequency in the simulated acceleration spectrum is 112.55Hz, while its experimental value is 113.30Hz. The outer planet rotation frequency in the simulated acceleration spectrum is 118.51Hz, while its experimental value is 118.70Hz. The simulated results are similar as the experimental results. Thus, the proposed dynamic model is correct.

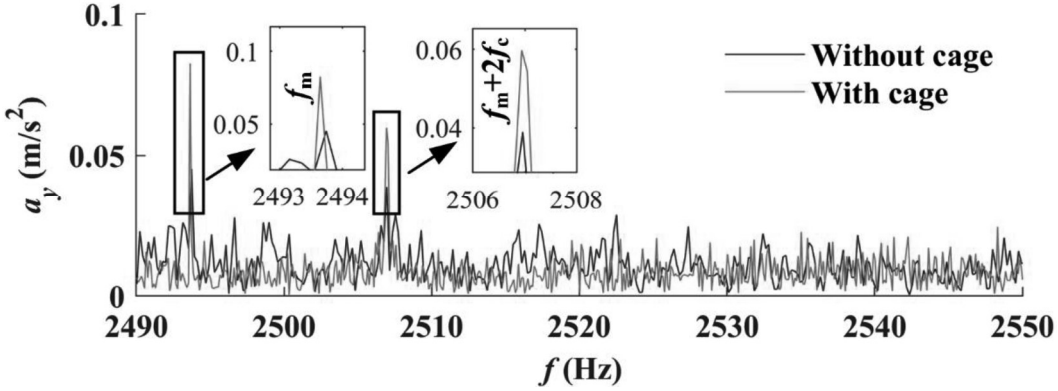

Fig. 22. Comparisons of the model with the cage (proposed model) and the one without the cage in the spectrum.

(a)

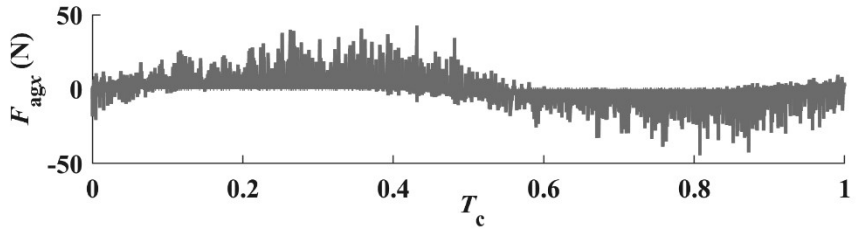

(b)

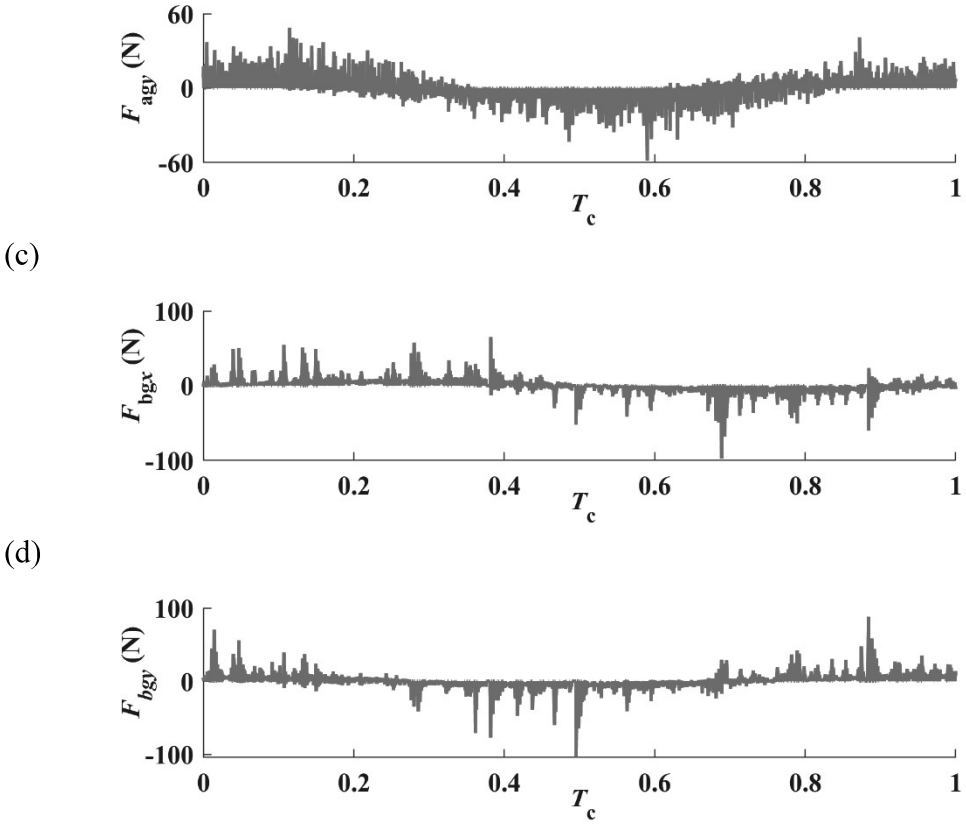

Fig. 23. The resultant forces of (a) inner planet-cage impact force and frictional force in x directions; (b) inner planet-cage impact force and frictional force in y directions; (c) outer planet-cage impact force and frictional force in x directions; and (d) outer planet-cage impact force and frictional force in y directions.

Fig. 22 gives the comparison of model with the cage (proposed model) and that without the cage in the spectrum. In Fig. 22, f_m and f_m+2f_c can be found for those with and without the cage models. The reason for the phenomenon is that the relative meshing phases of the planets are different. Thus, the meshing stiffness in the same angle position are different for different planet. Only when the planet rotates 180°, the DPGS will generate the same vibrations with the initial condition. On the other hand, the DPGS vibration spectrum will be modulated by $2f_c$. Thus, the frequency f_m+2f_c become more obvious in the spectrum. The values of f_m and f_m+2f_c are 2493.64 Hz; and that of proposed model is 2503.94 Hz; while those are 2493.74 Hz and 2506.96 Hz for the model without the cage. The experimental value of f_m is 2493.2 Hz, as shown in Fig. 21(b). The value of f_m obtained by the proposed model is closer to the experimental value than that obtained by the model without the cage. Moreover, the amplitudes of f_m and f_m+2f_c of proposed model are larger than those of model without the cage. The amplitudes of f_m and f_m+2f_c of proposed model are 0.0827 m/s^2 and 0.0598 m/s^2; while those of model without the cage are 0.0454 m/s^2 and 0.039 m/s^2. The amplitude of f_m for proposed model is 38.3% larger than that of model without the cage; and the amplitude of f_m+2f_c for proposed model is 16.4% larger than that of model without the cage. This is because the proposed model considers the roller-cage impact force and cage vibrations, which will affect the gear rotation velocities and vibrations. Moreover, as shown in Fig. 23 and Fig. 6, the resultant forces of planet-cage impact force and

frictional force are still not small values compared with the contact forces. Thus, the planet-cage impact force and frictional force will have a non-negligible effect on the DPGS vibrations. In addition, the planet-cage frictional force will have a significant effect on the planetary bearing sliding rate, which will also generate effect on the DPGS vibrations. These indicate that the cage has a significant effect on the DPGS vibrations. On the other hand, these indicate that the proposed model is more accurate.

5. Conclusions

This work proposes a dynamic model for vibration analysis of the planetary bearing in DPGS. The proposed model considers the planetary bearing roller and cage dynamic characteristics. Moreover, the gear interactions, planetary gear-bearing-carrier interactions, and roller-cage interactions are contained in the proposed model. In comparison with the previous studies, this work establishes an improved dynamic model for a DPGS containing all components (sun gear, ring gear, carrier, inner planet, outer planet, planetary bearing roller, and planetary bearing cage). The components' excitations in this work are more comprehensive. An experiment is used to prove the correctness of the proposed model. The conclusions are summarized as follows:

(1) The planetary bearing contact force, roller-cage impact force, planetary bearing roller acceleration, planet acceleration, carrier acceleration, and planetary bearing cage acceleration exhibit obvious periodic variations. The contact force periodic frequency of inner planetary bearing approximately equal to f_{ga}-f_c and that of outer planetary bearing approximately equal to f_{ga}+f_c.

(2) The RMS and MAX values of planetary bearing contact force and roller-cage impact force generally increase with the increment of sun gear rotation speed.

(3) The RMS and MAX values of planetary bearing roller acceleration, planet roller acceleration, carrier roller acceleration, and planetary bearing cage roller acceleration generally increase with the increment of sun gear rotation speed.

(4) The simulated results are similar as the experimental results both in the time-domain and frequency-domain. The value of f_m obtained by the proposed model is closer to the experimental value than that obtained by the model without the cage. Moreover, the amplitudes of f_m and f_m+2f_c of proposed model are larger than those of model without the cage. Thus, the proposed dynamic model is correct.

Although the proposed model is more comprehensive than other models, it also has some aspects need to be improved. The planetary bearing cage has a big centrifugal force rotating about the planetary gear set axis. It will generate significant flexible deformation due to the cage-planet impact, which will affect the cage-planet contact stiffness and cause the change of DPGS vibrations. Moreover, the effect of the gear backlash on the DPGS vibrations are ignored in this work. However, the gear backlash is an important excitation source for DPGS and has a significant effect on the DPGS vibrations. Therefore, the cage flexibility and gear backlash need to be considered in the future work.

Funding

Support provided by the National Natural Science Foundation of China under Contract No. 52175120, 51975068 and 5211101862.

Conflict of Interest

The author declared that he has no conflicts of interest.

[1] Wei L, Kai S, Hailong S, et al. Modulation sideband analysis of a two-stage planetary gear system with an elastic continuum ring gear. Journal of Sound and Vibration, 2022, 527: 116874.

[2] Duan T, Wei J, Yan Q, et al. Investigations on crack propagation and meshing characteristics

of planetary gear train considering crack closure effect. Engineering Failure Analysis, 2022: 106064.
[3] Kahraman A. Free torsional vibration characteristics of compound planetary gear sets. Mechanism and machine theory, 2001, 36(8): 953-971.
[4] Bahk C J, Parker R G. Analytical solution for the nonlinear dynamics of planetary gears. Journal of Computational and Nonlinear Dynamics, 2011, 6(2): 021007.
[5] Bahk C J, Parker R G. Analytical investigation of tooth profile modification effects on planetary gear dynamics. Mechanism and machine theory, 2013, 70: 298-319.
[6] Öztürk V Y, Cigeroglu E, Özgüven H N. Ideal tooth profile modifications for improving nonlinear dynamic response of planetary gear trains. Journal of Sound and Vibration, 2021, 500: 116007.
[7] Fatourehchi E, Mohammadpour M, King P D, et al. Effect of mesh phasing on the transmission efficiency and dynamic performance of wheel hub planetary gear sets. Journal of Mechanical Engineering Science, 2018, 232(19): 3469-3481.
[8] Chen Z, Shao Y. Dynamic simulation of planetary gear with tooth root crack in ring gear. Engineering Failure Analysis, 2013, 31: 8-18.
[9] Shen Z, Qiao B, Yang L, et al. Fault mechanism and dynamic modeling of planetary gear with gear wear. Mechanism and Machine Theory, 2021, 155: 104098.
[10] Xiang L, Gao N, Hu A. Dynamic analysis of a planetary gear system with multiple nonlinear parameters. Journal of Computational and Applied Mathematics, 2018, 327: 325-340.
[11] Luo W, Qiao B, Shen Z, et al. Investigation on the influence of spalling defects on the dynamic performance of planetary gear sets with sliding friction. Tribology International, 2021, 154: 106639.
[12] K Khoozani M, Poursina M, P Anaraki A. Study of gyroscopic effects on the dynamics and vibrations of double-helical planetary gear set. Journal of Multi-body Dynamics, 2018, 232(2): 199-223.
[13] Kim W, Lee J Y, Chung J. Dynamic analysis for a planetary gear with time-varying pressure angles and contact ratios. Journal of Sound and Vibration, 2012, 331(4): 883-901.
[14] Xu Z, Yu W, Shao Y, et al. Dynamic modeling of the planetary gear set considering the effects of positioning errors on the mesh position and the corner contact. Nonlinear Dynamics, 2022: 1-19.
[15] Hu A, Liu S, Xiang L, et al. Dynamic modeling and analysis of multistage planetary gear system considering tooth crack fault. Engineering Failure Analysis, 2022: 106408.
[16] Wang P, Xu H, Ma H, et al. Effects of three types of bearing misalignments on dynamic characteristics of planetary gear set-rotor system. Mechanical Systems and Signal Processing, 2022, 169: 108736.
[17] Guo Y, Parker R G. Dynamic analysis of planetary gears with bearing clearance. Journal of Computational and Nonlinear Dynamics, 2012, 7(4): 041002.
[18] Liu J, Ding S, Wang L, et al. Effect of the bearing clearance on vibrations of a double-row planetary gear system. Journal of Multi-body Dynamics, 2020, 234(2): 347-357.
[19] Liu J, Pang R, Ding S, et al. Vibration analysis of a planetary gear with the flexible ring and planet bearing fault. Measurement, 2020, 165: 108100.
[20] Liu J, Xu Y, Shao Y, et al. The effect of a localized fault in the planet bearing on vibrations of a planetary gear set. Journal of Strain Analysis for Engineering Design, 2018, 53(5): 313-323.
[21] Denni M, Biboulet N, Abousleiman V, et al. Dynamic study of a roller bearing in a planetary application considering the hydrodynamic lubrication of the roller/cage contact. Tribology International, 2020, 149: 105696.

[22] Moshrefzadeh A, Fasana A. Planetary gearbox with localised bearings and gears faults: simulation and time/frequency analysis. Meccanica, 2017, 52(15): 3759-3779.
[23] Liu Y Q, Chen Z G, et al. Surface wear evolution of traction motor bearings in vibration environment of a locomotive during operation. SCIENCE CHINA -Technological Sciences, 2022, 65(4), 920-931.
[24] Liu Y Q, Chen Z G, et al. Skidding dynamic performance of rolling bearing with cage flexibility under accelerating conditions. Mechanical Systems and Signal Processing 150 (2021) 107257.
[25] Wu W, Wei C, Yuan S. Numerical simulation of ball bearing flow field using the moving particle semi-implicit method. Engineering Applications of Computational Fluid Mechanics, 2022, 16(1): 215-228.
[26] Liang X H, Zuo M J, Guo Y M. Evaluating the time-varying mesh stiffness of a planetary gear set using the potential energy method. Proceedings of the 7th World Congress on Engineering Asset Management (Wceam 2012). 2015, 365-374.
[27] Liu J, Li X, Ding S, et al. A time-varying friction moment calculation method of an angular contact ball bearing with the waviness error. Mechanism and Machine Theory, 2020, 148: 103799.
[28] Lei Y, Luo X, Liu Z, et al. A new dynamic model of planetary gear sets and research on fault response characteristics. Journal of Mechanical Engineering, 2016, 52(13): 111-122.

Appendix A: Calculation method for the vibration contribution coefficients

$$y_{\mathrm{p}}=\sum_{k=1}^{N_{\mathrm{t}}}\left(\mathrm{RMS}\left(a_{\mathrm{p}k}\right)+\mathrm{MAX}\left(a_{\mathrm{p}k}\right)\right) \tag{1}$$

where, $a_{\mathrm{p}k}$ is the simulated acceleration signals of k-th work condition, N_{t} is the number of working conditions of calculation group.

$$y_{\mathrm{t}}=\sum_{k=1}^{N_{\mathrm{t}}}\left(\mathrm{RMS}\left(a_{tk}\right)+\mathrm{MAX}\left(a_{tk}\right)\right) \tag{2}$$

where, $a_{\mathrm{p}k}$ is the experimental acceleration signals of k-th work condition.

$$f=\left|y_{\mathrm{p}}-y_{\mathrm{t}}\right| \tag{3}$$

The vibration contribution coefficients can be obtained by finding the minimum value of f, the problem can be expressed by

$$\min_{x} f\left(x\right) \text{ such that } \begin{cases} x\left(1\right)-x\left(2\right)=0 \\ 0\le x\le 1 \end{cases} \tag{4}$$

$$x=\left[C_{\mathrm{a}} \quad C_{\mathrm{b}} \quad C_{\mathrm{c}} \quad C_{\mathrm{s}} \quad C_{\mathrm{r}}\right] \tag{5}$$

Then using the validation group signals to verify the correctness of the vibration contribution coefficients

$$\hat{y}_{\mathrm{p}}=\sum_{k=1}^{N_{\mathrm{c}}}\left(\mathrm{RMS}\left(a_{\mathrm{p}k}\right)+\mathrm{MAX}\left(a_{\mathrm{p}k}\right)\right) \tag{6}$$

$$\hat{y}_{\mathrm{t}}=\sum_{k=1}^{N_{\mathrm{c}}}\left(\mathrm{RMS}\left(a_{tk}\right)+\mathrm{MAX}\left(a_{tk}\right)\right) \tag{7}$$

where, N_c is the number of working conditions of the validation group.

$$\text{rel}=\frac{\left|\hat{y}_{\text{p}}-\hat{y}_{\text{t}}\right|}{\hat{y}_{\text{t}}} \tag{8}$$

If rel<0.15, the obtained vibration contribution coefficients can be recognized as correct.